Local Protein Dynamics during Microvesicle Exocytosis in Neuroendocrine Cells

Agila Somasundaram[1] and Justin W. Taraska[1, 2]

Running title: Protein dynamics at fusing vesicles

Abbreviations: SV, synaptic vesicle; SLMV, synaptic-like microvesicle; LDCV, large dense core vesicle; TIRF, total internal reflection fluorescence microscopy; CME, clathrin-mediated endocytosis

[1]Laboratory of Molecular Biophysics, 50 South Drive, Building 50, National Heart, Lung, and Blood Institute, National Institutes of Health, Bethesda, MD 20892
[2]Corresponding author; justin.taraska@nih.gov

ABSTRACT

Calcium triggered exocytosis is key to many physiological processes, including neurotransmitter and hormone release by neurons and endocrine cells. Dozens of proteins regulate exocytosis, yet the temporal and spatial dynamics of these factors during vesicle fusion remain unclear. Here we use total internal reflection fluorescence microscopy to visualize local protein dynamics at single sites of exocytosis of small synaptic-like microvesicles in live cultured neuroendocrine PC12 cells. We employ two-color imaging to simultaneously observe membrane fusion (using vesicular acetylcholine transporter (VAChT) tagged to pHluorin) and the dynamics of accessory proteins at the moments surrounding exocytosis. Our experiments reveal that many proteins, including the SNAREs syntaxin1 and VAMP2, the SNARE modulator tomosyn, and Rab proteins, are pre-clustered at fusion sites and rapidly lost at fusion. The ATPase NSF is recruited at fusion. Interestingly, the endocytic BAR domain-containing proteins amphiphysin1, syndapin2, and endophilins are dynamically recruited to fusion sites, and slow down the release of vesicle membrane-bound cargo. A similar effect on cargo release was seen with the over-expression of the GTPases dynamin1 and dynamin2. These results suggest that proteins involved in classical clathrin-mediated endocytosis regulate exocytosis of synaptic-like microvesicles, possibly by modulating the highly curved neck of the vesicle fusion pore. Our findings provide insights into the dynamics, assembly, and mechanistic roles of many key modulators of exocytosis and endocytosis at single sites of microvesicle fusion in live cells.

INTRODUCTION

Exocytosis is the cellular process in which cytoplasmic membrane-bound vesicles fuse with the plasma membrane and release their contents into the extracellular space. During synaptic transmission, action potentials depolarize the presynaptic terminal triggering Ca^{2+} influx into the cell. Local elevations in intracellular Ca^{2+} cause synaptic vesicles (SVs) in the terminal to fuse with the plasma membrane releasing neurotransmitters into the synaptic cleft (Jahn and Fasshauer, 2012). SV exocytosis is a carefully orchestrated cellular process that involves multiple steps and dozens of proteins. SVs are small, ~ 40 nm in diameter, and contain a small repertoire of proteins on their membranes (Takamori et al., 2006). These vesicular proteins and several cytoplasmic and membrane-associated proteins play important roles in regulating SV exocytosis (Sudhof, 2013d).

Specifically, SNARE proteins are thought to drive SV fusion with the plasma membrane (Sudhof and Rothman, 2009). The vesicular SNARE, synaptobrevin (VAMP), and the plasma membrane SNAREs, syntaxin and SNAP-25, form a four-helical zippered complex that pulls the two lipid bilayers together resulting in fusion. The SNAREs are sufficient for fusion in vitro (van den Bogaart et al., 2010). However, under physiological conditions, several proteins such as Rabs and their effector molecules (Fukuda, 2008), complexin (Trimbuch and Rosenmund, 2016), the Ca sensor synaptotagmin (Sudhof, 2013a), tomosyn (Ashery et al., 2009; Bielopolski et al., 2014), CAPS (Stevens and Rettig, 2009), Munc18 and Munc13 (Sudhof and Rothman, 2009) have been proposed to regulate the steps leading to fusion, including docking (attaching the SV to the active zone) and priming (preparing the SV for fusion) (Sudhof, 2013d). While much is known about the biochemical properties of these proteins, a comprehensive understanding of their spatial and temporal dynamics during exocytosis of SVs in live cells is lacking, partly due to their small size and the challenges associated with labeling and imaging single vesicles (Kavalali and Jorgensen, 2014). Understanding the dynamics of key mediators of SV exocytosis will provide direct insights into their regulatory functions, biological mechanisms, and roles in disease.

Here, we used total internal reflection fluorescence (TIRF) microscopy to monitor the dynamics of over two dozen proteins during calcium-triggered exocytosis of single synaptic-like microvesicles (SLMVs) in PC12 neuroendocrine cells. SLMVs or microvesicles are structurally and functionally similar to neuronal SVs (Thomas-Reetz and De Camilli, 1994). These small vesicles maintain an acidic pH, accumulate chemicals and other hormones, and fuse with the plasma membrane to release their luminal contents in a Ca^{2+}-dependent manner. Aside from the interest in their intrinsic biological functions in endocrine cells, these vesicles have been used as experimentally tractable surrogates for the study of SV behavior (de Wit et al., 2001; Sochacki et al., 2012). In an imaging-based screen examining several key exocytic and endocytic proteins, we show that many proteins, including SNAREs, tomosyn, and Rab GTPases are pre-clustered at fusion sites and rapidly diffuse away following fusion. Interestingly, BAR domain-containing proteins, and dynamin, known to be important in clathrin-mediated endocytosis, are recruited to exocytic sites and influence the release of vesicle membrane proteins into the plasma membrane. Our study provides insights into the local dynamics, assembly, and function of key regulators of exocytosis and endocytosis during microvesicle fusion in live cells.

RESULTS

To image microvesicle fusion in PC12 cells, we expressed the vesicular acetylcholine transporter (VAChT) tagged on its luminal side to pHluorin, a pH-sensitive variant of green fluorescent protein (Miesenbock et al., 1998). VAChT is targeted specifically to synaptic-like microvesicles (SLMVs) in PC12 cells (Liu and Edwards, 1997), and VAChT-pHluorin has been used to track SLMV exocytosis (Brauchi et al., 2008; Sochacki et al., 2012). pHluorin fluorescence is quenched in the acidic lumen of the vesicle, but upon fusion the luminal pH is neutralized by the extracellular buffer causing pHluorin signal to dramatically increase, enabling the detection of exocytic events. To stimulate exocytosis, we depolarized cells by applying buffer containing high extracellular KCl using a superfusion pipette positioned close to the cell (Trexler et al., 2016; Trexler and Taraska, 2017). Membrane depolarization-induced fusion events were detected as sudden bright flashes of green fluorescence (Fig. 1A). This is observed as a local sharp increase in signal that decays with time as VAChT-pH diffuses away from the sites of exocytosis (Fig. 1A, bottom). In the red fluorescent channel, we monitored co-expressed proteins fused to mCherry, mRFP or mKate2 (Supp. Table 1). In the example shown in Fig. 1, VAChT-pH was co-expressed with mRFP-Rab3A (Fig. 1B), where measurable changes in signal were detected during fusion (Fig. 1B, bottom). Background-subtracted and normalized fluorescence intensities from hundreds of individual fusion events were extracted, normalized, and averaged in the green and red channels for every protein examined in the study to produce the average time-dependent changes in protein signals at fusion sites (Fig. 1C, D). We analyzed ~ 8,000 fusion events from over 300 cells to track, quantitate, and characterize the dynamics of dozens of proteins (Supp. Table 1) during exocytosis of microvesicles.

Rab GTPases and effectors are rapidly lost from sites of SLMV exocytosis

We first examined the dynamics of the Rab family of GTPases and Rab effector molecules, which play important roles in targeting and docking synaptic vesicles to the plasma membrane (Fukuda, 2008) during SLMV exocytosis in PC12 cells. Rab27A and Rab3A were localized at exocytic sites before fusion and diffused away rapidly following exocytosis, consistent with their vesicle membrane-anchored nature (Fig. 2A, B, Supp. Fig. 2). The cytosolic Rab3A effector molecule, Rabphilin3A, also displayed similar localization and behavior (Fig. 2C, Supp. Fig. 2). Rab5A, an early endosomal Rab (Woodman, 2000), showed some enrichment at fusion sites, that slowly decreased following fusion (Fig. 2D, Supp. Fig. 2). Rab27B did not exhibit specific localization at SLMVs (Supp. Fig. 2) or change in intensity following fusion (Fig. 2E). These results demonstrate that the Rab proteins, Rab27A and Rab3A, and the effector Rabphilin3A, are enriched at microvesicle sites before exocytosis and are dynamically lost into the cytosol or plasma membrane following fusion.

SNAREs, syntaxin1 and VAMP2, are clustered at fusion sites and lost following fusion

Docked vesicles fuse with the plasma membrane by the concerted action of the SNARE proteins syntaxin, SNAP25 and VAMP2(Sudhof and Rothman, 2009). We found that the plasma membrane SNARE, syntaxin1, decreased in intensity at fusion sites during exocytosis (Fig. 3A). Examination of average syntaxin1 fluorescence intensities before, during, and after fusion revealed locally elevated syntaxin1 that diffused away following fusion, indicating that syntaxin1 is clustered on the plasma membrane at sites of microvesicle exocytosis (Supp. Fig. 2) (Barg et al., 2010; Gandasi and Barg, 2014; Lang et al., 2001; Ullrich et al., 2015). We did not observe re-clustering of

syntaxin1 at the original fusion sites within 5 s of fusion (Supp. Fig. 2). The plasma membrane-attached SNARE, SNAP25, did not exhibit a substantial change in signal (Fig. 3B) or distribution (Supp. Fig. 9) during fusion. VAMP2 showed some concentration at fusion sites (Supp. Fig. 2), consistent with its expression on the vesicular membrane, and diffused away following fusion (Fig. 3C). To rule out potential artifacts induced by the red fluorescent tag, we examined the distribution and dynamics of cytosolic mCherry and membrane-attached farnesyl-mCherry during fusion. Cytosolic mCherry was diffusely distributed both before and during fusion (Supp. Fig. 2), and did not show substantial changes in signal during fusion (Fig. 3D). The small increase in signal seen several seconds later could be due to mCherry diffusing into the cytosolic space now made available by the fused vesicle (Taraska et al., 2003). Farnesyl-mCherry signal increased slightly during fusion (Fig. 3E), perhaps due to incorporation of the vesicle membrane into the plasma membrane, and is reflected in the average images as a small local increase at fusion sites (Supp. Fig. 2). Thus, the control mCherry proteins exhibited small or no changes in signal during fusion that are markedly different from the dynamics of syntaxin1 and VAMP2 described above (Fig. 3A, C). In conclusion, the SNAREs syntaxin1 and VAMP2 are locally pre-assembled at microvesicle exocytic sites and diffuse away from the site of release.

SNARE modulators exhibit diverse behaviors during SLMV fusion

SNARE-mediated fusion is regulated by several proteins (Sudhof, 2013d). To gain insights into the function of these SNARE modulators in cells, we next examined their dynamics during SLMV fusion in PC12 cells. Multiple roles have been proposed for the small protein complexin, which is thought to either clamp the SNARE complex in a partially zippered state, or facilitate fusion (An et al., 2010; Brose, 2008; Wragg et al., 2013; Yoon et al., 2008). Complexin2 signal decreases slightly during fusion (Fig. 4A); however, most of the protein appeared diffusely distributed before and after fusion (Supp. Fig. 2). A small but non-significant decrease in signal was also seen with CAPS (Fig. 4B), a protein essential for SV priming (Jockusch et al., 2007). Unlike complexin2, CAPS displayed some preferential localization at fusion sites at rest, and more diffuse localization post-fusion (Supp. Fig. 2). The Ca sensor synaptotagmin1 (Sudhof, 2013a) was concentrated at fusion sites but, surprisingly, did not diffuse away following fusion (Supp. Fig. 1A, Supp. Fig. 2). Tomosyn, thought to play a largely inhibitory role in SV priming (Ashery et al., 2009; Bielopolski et al., 2014; Cazares et al., 2016; Gracheva et al., 2006; McEwen et al., 2006)was located as clusters at vesicles and diffused away following fusion (Fig. 4C). Munc18a and Munc13, proteins proposed to bind the SNAREs and have essential roles in SV fusion (Sudhof and Rothman, 2009), did not exhibit significant changes in dynamics during fusion (Supp. Fig. 1C, Supp. Fig. 2). Interestingly, the ATPase NSF was transiently recruited to fusion sites during exocytosis (Fig. 4C, Supp. Fig. 2), consistent with its role in disassembling SNARE complexes (Ryu et al., 2016). Overall, SNARE modulators exhibited diverse and subtle behaviors, with some pre-assembled at fusion sites and lost following fusion (CAPS and tomosyn), some recruited to fusion sites (NSF), and others localized at fusion sites throughout fusion (synaptotagmin1). These data likely reflect the diverse functions of these different classes of proteins along with the transient and dynamic nature of their activities at microvesicles during release.

BAR domain proteins are recruited to sites of SLMV exocytosis

Previous studies have shown that the proteins amphiphysin, syndapin, and dynamin, involved in the maturation and scission of clathrin-coated endocytic structures (Daumke et al., 2014; McMahon and Boucrot, 2011), are recruited to exocytic sites (Jaiswal et al., 2009; Trexler et al.,

2016; Tsuboi et al., 2004) and regulate Ca^{2+}-dependent cargo release from large dense core vesicles (LDCVs) in endocrine cells (Anantharam et al., 2011; Anantharam et al., 2010; Fulop et al., 2008; Graham et al., 2002; Holroyd et al., 2002; Llobet et al., 2008; Min et al., 2007; Samasilp et al., 2012; Trexler et al., 2016; Tsuboi et al., 2004), and constitutive secretion from post-Golgi vesicles (Jaiswal et al., 2009). Because SLMVs are 5-fold smaller than LDCVs and likely have different overall curvatures, we hypothesized that a distinct set of proteins might be involved (Xu and Xu, 2008; Zhang and Jackson, 2010). We first imaged the dynamics of the curvature sensing/inducing BAR domain proteins amphiphysin1 and syndapin2. Both proteins were diffusely localized at fusion sites, but were specifically recruited to microvesicle fusion sites during exocytosis (Fig. 5, Supp. Fig. 9). BAR domain proteins endophilinA1 and endophilinA2 were also recruited during fusion (Supp. Fig. 3A, B, Supp. Fig. 9). EndophilinB1, however, appeared localized at fusion sites even at rest (Supp. Fig. 9), and did not exhibit significant changes in dynamics during fusion (Supp. Fig. 3C). Overall, these results indicate that specific BAR domain proteins are recruited to SLMVs at exocytosis in neuroendocrine cells.

To determine if amphiphysin1 and syndapin2 recruitment to the site of fusion is driven by the curvature-sensitive BAR domains (Daumke et al., 2014), we imaged mutants lacking BAR domains. Unlike the wild-type (WT) proteins, Amph1-ΔBAR and Synd2-ΔBAR did not show specific localization at fusion sites during exocytosis (Fig. 6A-D, Supp. Fig. 9), indicating that the BAR domain is required for amphiphysin1 and syndapin2 recruitment. Deletion of the protein-protein interaction domain (SH3) (David et al., 1996; Grabs et al., 1997; Qualmann et al., 1999) in amphiphysin1 (Amph1-ΔSH3) and syndapin2 (Synd2-ΔSH3) did not prevent recruitment (Fig. 6E, F, Supp. Fig. 9), suggesting that the SH3 domain is not required for their localization to SLMVs during fusion. Moreover, the BAR domain of syndapin2 (Synd2-BAR) showed strong recruitment (Fig. 6H, Supp. Fig. 9), whereas over-expression of just the SH3 domain of amphiphysin1 (Amph1-SH3) did not show any recruitment to fusion sites (Fig. 6G, Supp. Fig. 9). Thus, amphiphysin1 and syndapin2 recruitment is dependent on the BAR domain, suggesting that these proteins are recruited to the highly curved neck of the expanding fusion pore. Interestingly, amphiphysin1 and syndapin2 proteins that showed strong recruitment (Amph1-WT, Amph1-ΔSH3, Synd2-WT, Synd2-BAR) were partially localized at fusion sites many seconds after fusion (Fig. 6, Supp. Fig. 9), suggesting the persistence of the curved neck of the pore. These data also suggest that amphiphysin1 and syndapin2 could have mechanistic roles in regulating the behavior of the expanding microvesicle fusion pore.

BAR domain proteins modulate SLMV membrane cargo release

We next investigated whether the recruitment of BAR domain proteins described above impacts SLMV fusion dynamics. We used the VAChT-pH fluorescence decay (Fig. 1C), which reflects the diffusion of released VAChT away from the sites of fusion (Sochacki et al., 2012), as a readout of the rate of vesicle membrane cargo release. Expression of Amph1-WT did not significantly alter VAChT-pH decay when compared with farnesyl-mCherry (Supp. Fig. 4A). However, over-expression of Amph1-ΔBAR and Amph1-SH3, proteins that were not recruited to fusion sites (Fig. 6C, G, Supp. Fig. 9), resulted in faster VAChT-pH decay when compared with WT (Fig. 7A), indicating a dilated fusion pore. On the other hand, over-expression of Amph1-ΔSH3, which was recruited to fusion sites (Fig. 6E, Supp. Fig. 9), resulted in even slower VAChT-pH release (Fig. 7A), suggesting a role for the SH3 domain in modulating the fusion pore. These results suggest

that amphiphysin1 recruitment during SLMV fusion slows the release of vesicle membrane proteins by narrowing or restricting the fusion pore.

We obtained similar results with syndapin2. Like Amph1-WT, expression of Synd2-WT did not alter VAChT-pH decay when compared with farnesyl-mCherry control (Supp. Fig. 4B). Synd2-ΔBAR, which was not recruited to fusion sites (Fig. 6D, Supp. Fig. 9), exhibited VAChT decay similar to Synd2-WT (Fig. 7B). However, Synd2-ΔSH3 and Synd2-BAR, which showed strong and specific recruitment to fusion sites (Fig. 6F, H, Supp. Fig. 9), substantially slowed down VAChT release (Fig. 7B). Thus, the lack of the SH3 domain in amphiphysin1 and syndapin2 further slows down fusion when compared with WT (Fig. 7A, B), suggesting a narrower pore. Furthermore, the BAR domain proteins, endophilinA1, endophilinA2 and endophilinB1, that showed recruitment or localization at fusion sites (Supp. Fig. 3, Supp. Fig. 9) resulted in significantly slower VAChT-pH decay when compared with farnesyl-mCherry (Supp. Fig. 5). Intriguingly, the VAChT-pH decay with farnesyl-mCherry was slower than with cytosolic mCherry (Supp. Fig. 4C). It is possible that the small increase in farnesyl-mCherry seen during exocytosis (Fig. 2E, Supp. Fig. 9) alters membrane properties including fluidity or packing to slow down cargo release (Stachowiak et al., 2012). Because we are interested in the impact of membrane-associated BAR domain proteins on fusion dynamics, we chose to compare their VAChT-pH decay profiles with that seen with farnesyl-mCherry (Supp. Fig. 4, Supp. Fig. 5). Overall, our results indicate that BAR domain proteins delay the release of vesicle membrane cargo during SLMV exocytosis, likely by narrowing or restricting the fusion pore.

As another test of this hypothesis, we examined the effects of knock-down of endogenous amphiphysin1 and syndapin2 on VAChT-pH release by treating cells with siRNA against these molecules. Western blot analysis revealed syndapin2 expression in PC12 cells, which was reduced with siRNA treatment (Supp. Fig. 6A). We were unsuccessful in our attempts to detect endogenous amphiphysin1 using commercial antibodies (data not shown). Contrary to our expectation, the VAChT-pH decay in PC12 cells treated with siSyndapin2 was slower than that with control siRNA (Supp. Fig. 6B). It is possible that syndapin2 knock-down resulted in increased recruitment of other BAR domain proteins to SLMVs, but we did not explore this further. Nonetheless, our experiments with amphiphysin1 and syndapin2 mutants, and endophilins, provide compelling evidence for the modulation of microvesicle membrane cargo release by BAR domain proteins.

Dynamin is recruited to fusion sites and alters SLMV cargo release

Expression of amphiphysin1 and syndapin2 mutants lacking the SH3 domains resulted in slower VAChT-pH release than that seen with full-length proteins (Fig. 7), suggesting a role for SH3 binding partners in hastening cargo release. To test this, we examined the dynamics of the well-studied SH3 binding partner, the GTPase dynamin (David et al., 1996; Ferguson and De Camilli, 2012; Qualmann et al., 1999). During clathrin-mediated endocytosis (CME), dynamin localizes to the curved neck of the invaginating clathrin-coated pit through its interactions with BAR domain proteins and causes scission (Daumke et al., 2014). Dynamin1 and dynamin2 have also been shown to cluster at LDCV fusion sites (Holroyd et al., 2002; Trexler et al., 2016; Tsuboi et al., 2004), and regulate fusion pore expansion (Anantharam et al., 2011; Fan et al., 2015; Fulop et al., 2008; Gonzalez-Jamett et al., 2013; Holroyd et al., 2002; Min et al., 2007; Samasilp et al., 2012; Trexler et al., 2016; Tsuboi et al., 2004). We found that dynamin1 is transiently recruited to SLMVs during fusion (Supp. Fig. 7A), and slows down VAChT-pH release (Fig. 8A). This suggests that

dynamin1 recruitment to SLMVs prevents the full expansion of the fusion pore resulting in slower cargo release. Dyn1-K44A, a GTPase mutant, was recruited to SLMV fusion sites (Supp. Fig. 7B), suggesting that the GTPase activity of dynamin1 is dispensable for its recruitment to SLMVs. Dyn1-K44A, however, hastened VAChT-pH decay when compared with Dyn1-WT (Fig. 8B). Thus, the recruitment of functional dynamin1 to SLMVs narrows the fusion pore slowing cargo release.

We next examined the effects of disrupting dynamin1's interactions with BAR domain proteins by mutating residues in its proline rich domain (PRD) (Okamoto et al., 1997). Dyn1 deficient in binding amphiphysin1 (Dyn1-833-838A, Dyn1-ΔAmph1) (Grabs et al., 1997) did not show specific localization at fusion sites, whereas dynamin1 deficient in binding syndapin2 (Dyn1-S774E/S778E, Dyn1-ΔSynd2) (Anggono et al., 2006) was recruited to SLMVs during fusion (Supp. Fig. 7C, D, Supp. Fig. 9). Both mutants, however, resulted in VAChT-pH decay that was comparable to that observed with Dyn1-WT (Fig. 8B), and slower than that with farnesyl-mCherry (Fig. 8A). It is possible that background levels of expression of Dyn1-ΔAmph1 was sufficient to affect VAChT release. Thus, our findings suggest that dynamin1 slows down membrane cargo release, and disrupting its interactions with either amphiphysin1 or syndapin2 does not diminish its effects on fusion.

Unlike Dyn1-WT (Supp. Fig. 7A), dynamin2 (Dyn2-WT) did not show significant recruitment to fusion sites (Supp. Fig. 7E). PC12 cells expressing Dyn2-WT, however, exhibited slower VAChT-pH decay when compared with farnesyl-mCherry (Fig. 8C). The strong effect of Dyn2-WT on VAChT-pH release suggests that low levels of Dyn2-WT at fusing vesicles can affect cargo release, or that dynamin2 acts at a step prior to exocytosis. Dynamin2 lacking the PRD domain (Dyn2-ΔPRD) resulted in faster release of cargo (Fig. 7D), suggesting that dynamin2's interaction with BAR domain proteins is essential for slowing down SLMV cargo release. Taken together, these results suggest that dynamin1 and dynamin2 slow the dilation of SLMV fusion pore resulting in slower cargo release. This is consistent with the observation that Amph1-SH3, which sequesters SH3 binding partners such as dynamin (Holroyd et al., 2002; Shupliakov et al., 1997; Wigge et al., 1997), results in faster VAChT-pH decay (Fig. 7A). These results also suggest that the slower VAChT-pH decay seen in Amph1-ΔSH3 and Synd2-ΔSH3 mutants (Fig. 7A, B) lacking dynamin binding is likely due to a lack of interactions with SH3 binding partners other than dynamin.

We next examined the dynamics of N-WASP, a regulator of CME that binds SH3-domain containing proteins such as amphiphysin and syndapin, and stimulates actin polymerization (Kessels and Qualmann, 2002; Qualmann et al., 1999; Yamada et al., 2009). We did not see significant changes in N-WASP signal (Supp. Fig. 8A), its distribution during fusion (Supp. Fig. 9), or the VAChT-pH decay profile when compared with controls (Supp. Fig. 8B). The adaptor protein AP-2 and the scaffolding protein intersectin also did not show significant changes in signal or distribution during fusion (Supp. Fig. 8C, D, Supp. Fig. 9). Interestingly, we observed a slow, but significant increase in clathrin around fusion sites several seconds after fusion (Supp. Fig. 8D, Supp. Fig. 9). Moreover, apart from the specific and transient recruitment of amphiphysin1 to fusion sites described earlier (Fig. 5, 6), in 5 out of 9 cells we observed a strong increase in amphiphysin1 clusters at the plasma membrane that peaked tens of seconds after stimulation and then disappeared (Supp. Fig. 10), suggesting compensatory endocytosis of released cargo

controlled by amphiphysin. Overall, our results suggest that BAR domain proteins and dynamin play important roles in modulating microvesicle fusion dynamics in endocrine cells.

DISCUSSION

Calcium-triggered exocytosis of SVs is a highly coordinated process involving dozens of proteins. The dynamics and assembly of these factors in live cells is not fully understood. In this study, we systematically analyzed the spatial and temporal dynamics of two dozen proteins at the moment of fusion of single SLMVs in living cells. Our experiments reveal distinct local dynamics of exocytic and endocytic factors, and a key role for BAR domain-containing proteins, along with dynamin, in directly modulating the microvesicle fusion pore.

First, we show that many key proteins involved in SV exocytosis are concentrated at fusion sites several seconds before fusion (Barg et al., 2010; Gandasi and Barg, 2014; Geerts et al., 2017; Lang et al., 2001; Trexler et al., 2016; Tsuboi and Rutter, 2003; Ullrich et al., 2015). These include the SNAREs, VAMP2 and syntaxin1 (Fig. 3), the Ca sensor synaptotagmin1 (Supp. Fig. 1), the SNARE modulators tomosyn and CAPS (Fig. 4), Rab proteins, Rab3A and Rab27A, and the rab effector molecule Rabphilin3A (Fig. 2) (Supp. Fig. 2). Because Rab proteins and VAMP2 are associated with the vesicle membrane, their presence before fusion indicates that SLMVs are docked at the plasma membrane prior to exocytosis. We did not measure additional recruitment of these molecules before fusion, suggesting that many proteins needed in exocytosis are pre-assembled at the vesicle. All these factors, except for synaptotagmin1, diffused away within seconds of fusion (Figs. 2-4, Supp. Fig. 1, Supp. Fig. 2), indicating the highly dynamic and transient nature of the complex.

Synaptotagmin1 remained localized at fusion sites after fusion (Supp. Fig. 1, 2), raising the possibility that SLMV fusion is incomplete. The complete release of VAChT-pH (Fig. 1), suggests that classic kiss-and-run (Alabi and Tsien, 2013) is not the predominant mode of SLMV exocytosis in PC12 cells (Sochacki et al., 2012). The residual VAChT-pH signal results from VAChT trapped in neighboring clathrin structures (Sochacki et al., 2012). We cannot, however, rule out a cavicapture-type fusion mechanism (Holroyd et al., 2002; Taraska et al., 2003; Tsuboi et al., 2004), where VAChT-pH is completely lost, but other components such as synaptotagmin1 are retained at fusion sites. Previous reports have suggested that synaptotagmin stays clustered after SV exocytosis (Willig et al., 2006). Given that synaptotagmin1 is an important cargo for clathrin-mediated endocytosis, it is possible that it is internalized very close to fusion sites through interactions with local adaptor proteins (Haucke and De Camilli, 1999; Martina et al., 2001; McMahon and Boucrot, 2011). This is supported by the slow increase in clathrin and the wave of amphiphysin1 recruitment to the plasma membrane observed many seconds after fusion (Supp. Figs. 8-10), and with previous studies demonstrating spatial and temporal proximity of exocytosis and compensatory endocytosis (Roos and Kelly, 1999; Sochacki et al., 2012; Wu et al., 2014).

We did not see clusters, or changes in dynamics of SNAP25 at fusion sites (Supp. Fig. 2, Fig. 3). It is possible that high levels of endogenous SNAP25 prevent the concentration of over-expressed or labeled protein at fusion sites (Knowles et al., 2010). Surprisingly, we also did not see significant changes in signal for Munc18a and Munc13 (Supp. Fig. 1, 2), molecules thought to be critical for vesicle docking and priming (Gandasi and Barg, 2014; Sudhof and Rothman, 2009), though

Munc18a proteins showed mild clustering at fusion sites (Supp. Fig. 2). Munc18a constructs with diminished promoter activity to reduce background signal also failed to show changes during fusion (not shown). Detecting small transient dynamics of all proteins during fusion in this system could require future technical developments.

Of note, we found that the ATPase NSF is recruited at exocytosis (Fig. 4). NSF and its binding partner α-SNAP (Ryu et al., 2016; Sollner et al., 1993; Ungermann et al., 1998) are thought to disassemble the SNARE complexes into monomeric SNAREs making them available for subsequent rounds of fusion (Ryu et al., 2016). It's unclear if NSF acts after fusion (Littleton et al., 2001), or immediately prior to fusion (Banerjee et al., 1996; Kuner et al., 2008). Here, the NSF signal appears to increase at fusion sites near the beginning of fusion (Fig. 4), and stays elevated for ~ 2 seconds, suggesting that NSF action is tightly coupled to microvesicle exocytosis, both spatially and temporally.

Importantly, we show that curvature sensing BAR domain proteins and the GTPase dynamin are locally recruited to SLMV fusion sites. Specifically, we measure dynamic recruitment of amphiphysin1, syndapin2, endophilinA1, endophilinA2 and dynamin1 to SLMVs during fusion (Fig. 5, 6, Supp. Figs. 3, 7, 9). EndophilinB1 appeared pre-clustered at fusion sites (Supp. Fig. 9), consistent with previous findings suggesting association of endophilins with SVs at rest in nerve terminals (Bai et al., 2010). Amphiphysin1 and syndapin2 recruitment was dependent on the BAR domain (Fig. 6) suggesting that these proteins are recruited to the curved membrane of the vesicle fusion pore.

Furthermore, we provide evidence that the presence of BAR domain proteins and dynamin at fusing SLMVs slows down the release of vesicle membrane cargo. Supporting this idea, over-expression of endophilinA1, endophilinA2, endophilinB1, dynamin1 and dynamin2 resulted in slower VAChT release (Supp. Fig. 5, Fig. 8). Second, amphiphysin1 mutants that failed to assemble at fusion sites resulted in faster release of proteins (Fig. 6, 7). Third, amphiphysin1 and syndapin2 mutants that lacked the SH3 domain but showed strong recruitment to fusion sites slowed down fusion (Fig. 6, 7). Fourth, dynamin1 lacking its GTPase activity, and fifth, dynamin2 deficient in binding BAR domain proteins, resulted in faster cargo release (Fig. 8). In total, the data supports a model where BAR domain proteins and dynamin act in concert to narrow the fusion pore restricting cargo release. It is also possible that these proteins have non-local effects on plasma membrane tension that affect fusion dynamics and diffusion of cargo (Stachowiak et al., 2012), but we haven't explored this further.

The slower cargo release seen with amphiphysin1 and syndapin2 mutants lacking the SH3 domain (Fig. 7) suggests that SH3 domain-binding partners could compensate for the narrowing of the pore by BAR domain proteins, and speed release. However, the prominent SH3 binding proteins dynamin1 and dynamin2 resulted in even further delays in protein release (Fig. 8), and N-WASP did not show significant recruitment, or affect cargo release (Supp. Figs. 8, 9), suggesting that interactions with other SH3 binding proteins (McPherson et al., 1994; McPherson et al., 1996), lipids (Martin, 2015), or rearrangements in the cytoskeleton (Felmy, 2007; Gonzalez-Jamett et al., 2017; Malacombe et al., 2006; Wen et al., 2016) may be involved in stabilizing the SLMV fusion pore.

Interestingly, the protein dynamics observed at SLMV fusion sites is like that seen with the much larger LDCVs in endocrine cells. While SVs and LDCVs have broadly similar molecular requirements for fusion (Xu and Xu, 2008), differences in their size (~ 40 nm vs. ~ 300 nm diameter), Ca^{2+} dependencies (Heidelberger et al., 1994; Sudhof, 2013a; Verhage et al., 1991), and latencies to fusion (Chow et al., 1992; Sabatini and Regehr, 1996), suggest differential regulation of the exocytic fusion machinery. Furthermore, their different curvatures, pore sizes (19 pS vs 213 pS conductance) (Klyachko and Jackson, 2002), and pore stabilities (Zhang and Jackson, 2010) suggest distinct structures of the pore. However, in both SLMVs and LDCVs, syntaxin1 (Barg et al., 2010; Gandasi and Barg, 2014; Lang et al., 2001), VAMP (Trexler et al., 2016; Tsuboi and Rutter, 2003), Rab3A (Gandasi and Barg, 2014; Trexler et al., 2016), Rab27A, Rabphilin3A, CAPS and tomosyn (Trexler et al., 2016) are concentrated at fusion sites, and diffuse away following fusion, supporting parallels in the molecular assembly and disassembly of key components during LDCV and microvesicle exocytosis. Moreover, BAR domain proteins and dynamin modulate fusion pore expansion in both SLMVs (Fig. 6, 7, Supp. Fig. 5) and LDCVs (Anantharam et al., 2011; Anantharam et al., 2010; Fulop et al., 2008; Holroyd et al., 2002; Llobet et al., 2008; Min et al., 2007; Trexler et al., 2016; Tsuboi et al., 2004). Specifically, in insulin-secreting beta cells, amphiphysin1, syndapin2, endophilinA2, dynamin1, and dynamin2 are recruited to LDCVs, and mutants of dynamin deficient in their interactions with BAR domain proteins hasten cargo release (Trexler et al., 2016). Given the different sensitivities to membrane curvature among the various BAR domain proteins (Daumke et al., 2014) and dynamin isoforms (Liu et al., 2011; Yoshida et al., 2004), the differences in their assembly and effects on LDCV and SLMV fusion kinetics may be nuanced.

Specifically, all three endophilins associated with SLMVs and slowed down cargo release (Supp. Figs. 3, 5, 9), whereas only endophilinA2 localizes with LDCVs (Trexler et al., 2016). Furthermore, dynamin delayed cargo release in SLMVs (Fig. 8), whereas in LDCVs, it is thought to cause vesicle scission (Tsuboi et al., 2004), enhance fusion pore dilation and cargo release (Anantharam et al., 2011), or slow down cargo release (Trexler et al., 2016). Additionally, dynamin1 mutants deficient in GTPase activity were shown to narrow the LDCV fusion pore (Anantharam et al., 2011; Tsuboi et al., 2004), which is different from our findings that dynamin1-K44A enhances cargo release from SLMVs (Fig. 8). It is possible that the failure of GTPase deficient dynamin to disassemble from membranes (Warnock et al., 1996) has different effects on fusion depending on the size or curvature of the vesicle. Future work at higher temporal or spatial resolutions comparing LDCVs and microvesicles in the same cells will help identify key differences in protein dynamics needed to regulate different pools of vesicles, their kinetics, and release of unique cargos.

At the neuronal synapse, the association of endocytic proteins with SVs is thought to ensure the availability of these proteins for compensatory endocytosis (Bai et al., 2010; Shupliakov, 2009). Our findings with SLMVs, which are structurally and functionally similar to SVs (Thomas-Reetz and De Camilli, 1994), suggest another function for endocytic proteins in directly impacting neurotransmitter release. The amount of neurotransmitter released by each fusing vesicle in the presynaptic cell depends on the neurotransmitter concentration, vesicle size, and whether the vesicle undergoes complete fusion or kiss-and-run (Ariel and Ryan, 2012). Modulating the expansion of the fusion pore by endocytic proteins offers a mechanism to fine-tune the rate or amount of cargo released (Chang et al., 2017; Guzman et al., 2010; Logan et al., 2017; Pawlu et

al., 2004), thereby influencing post-synaptic activity (Choi et al., 2003) or chemical signaling from endocrine cells.

MATERIALS AND METHODS

Cells and solutions

PC12-GR5 cells were grown in DMEM containing 4 mM L-glutamine, supplemented with 5% fetal bovine serum, 5% horse serum, and 1% penicillin/streptomycin, at 37 °C in 5% CO_2. The cell-line was obtained from Rae Nishi (OHSU), expanded from low passage frozen stocks, and was not further authenticated. The cells tested negative for mycoplasma contamination. Cells were plated onto 25-mm, #1.5, round, poly-D-lysine coated glass cover-slips, and transfected approximately 24–48 h later with 1 µg each of the indicated plasmids, or 25 nmol of siRNA (Dharmacon) using Lipofectamine 2000 (Invitrogen) following the manufacturer's protocol. The list of plasmids used and the n-values for all the experiments are in Supp. Table 1. Cells were imaged approximately 24-48 h after transfection. The imaging buffer contained (in mM): 130 NaCl, 2.8 KCl, 5 $CaCl_2$, 1 $MgCl_2$, 10 HEPES and 10 glucose. pH was adjusted to 7.4 with 1 N NaOH. The stimulation buffer contained (in mM): 50 NaCl, 105 KCl, 5 $CaCl_2$, 1 $MgCl_2$, 10 HEPES and 1 NaH_2PO_4. pH was adjusted to 7.4 with 5 M KOH.

TIRF microscopy

TIRF microscopy was done as previously described (Trexler et al, 2016; Trexler and Taraska, 2017). Cells were imaged on an inverted fluorescent microscope (IX-81, Olympus), equipped with a X100, 1.45 NA objective (Olympus). Combined green (488 nm) and red (561 nm) lasers (Melles Griot) were controlled with an acousto-optic tunable filter (Andor), and passed through a LF405/488/561/635 dichroic mirror. Emitted light was filtered using a 565 DCXR dichroic mirror on the image splitter (Photometrics), passed through 525Q/50 and 605Q/55 filters, and projected onto the chip of an EM-CCD camera. Images were acquired using the Andor IQ2 software. Cells were excited with alternate green and red excitation light, and images in each channel were acquired at 100 ms exposure, at 5 Hz. To trigger exocytosis, stimulation buffer was applied for 30 – 40 s using a µFlow perfusion system (ALA Scientific Instruments) with a 100 µm pipette positioned close to the surface of the cell. Each day before experiments, 100 nm yellow-green fluorescent beads (Invitrogen) were imaged in the green and red channels, and superimposed by mapping corresponding bead positions. The green and red cell images were aligned post-acquisition using projective image transformation as described before (Sochacki et al, 2012; Trexler et al, 2016). All experiments were carried out at 25 °C.

Image analysis

Image analysis was performed using Metamorph (Molecular Devices), ImageJ (NIH) and custom scripts on MATLAB (Mathworks). The co-ordinates of the brightest pixel in the first frame of brightening (fusion) for individual fusion events in the green channel were identified by eye, and assigned as the center of the fusion event. All events were time-aligned to the first frame of fusion (0 seconds). A circular ROI of 6 pixels (~ 990 nm) diameter and a square of 21 pixels (~ 3.5 µm) were drawn around the center, and the mean intensities in the surrounding square (background) were subtracted from the mean intensities in the center for each fusion event. This analysis was done for every frame from – 10 s to + 50 s. The background subtracted time-lapse intensities in the green channel were normalized 0 to 1 for each event, with '0' being the mean pre-fusion value,

obtained from -5 s to -3 s, and '1' being the peak intensity. The background subtracted time-lapse intensities for each event in the red channel were also normalized 0 to 1, with '0' being the minimum value, and '1' the maximum value, within – 10s to + 50 s. The resulting normalized traces were averaged across all events, and truncated to depict data from -5 seconds to +10 seconds to better represent the protein dynamics happening around the moment of fusion. The average images shown in Supp. Figs. 2 and 9 were obtained by averaging background subtracted frames from time-points indicated in figure legends. Fusion events were excluded from analysis if one or more additional fusion events occurred in the circular ROI within 5 seconds before or after fusion (-5 s to 5 s in the time-lapse traces).

Western Blots

PC12 cells were transfected with Syndapin2-GFP, or siRNA (Dharmacon) using Lipfectamine 2000, and protein was isolated ~ 24 h later. Cells were lysed in RIPA buffer (1 % Nonidet P-40, 0.5 % sodium deoxycholate, 0.1 % SDS and 1mM phenylmethylsulfonyl fluoride in PBS) on ice for 30 min. Lysates were centrifuged at 12,000g at 4°C for 10 min. Supernatants were boiled in lithium dodecyl sulphate (LDS) sample buffer containing 62.5 mM dithiothreitol for 10 min, and loaded onto 4-12 % Tris-Bis gels (NuPAGE). Protein was transferred onto nitrocellulose membrane using the iBlot dry transfer system (ThermoFisher Scientific), and syndapin2 detected with monoclonal antibody (ThermoFisher Scientific), and peroxidase-labelled secondary antibody. Blots were stripped with stripping buffer (ThermoFisher Scientific), and re-probed with α-actin antibody (Abcam).

Statistical Tests

All data are expressed as mean ± SEM. Statistical analysis was done using two-tailed paired or unpaired Student's t-test as indicated in figure legends. $p < 0.01$ was used as a measure of statistical significance.

ACKNOWLEDGEMENTS

We thank Marie-Paule Strub (NIH) for assistance with molecular biology, J. Silver, K. Sochacki and A. Trexler for critical reading of the manuscript, and members of the Taraska laboratory for discussions. J.W.T. is supported by the Intramural Research Program of the National Heart, Lung, and Blood Institute, National Institutes of Health.

AUTHOR CONTRIBUTIONS

A.S. and J.W.T. designed study, A.S. performed experiments and analyzed data, and A.S. and J.W.T. wrote the manuscript.

REFERENCES

Alabi, A.A., and R.W. Tsien. 2013. Perspectives on kiss-and-run: role in exocytosis, endocytosis, and neurotransmission. *Annu Rev Physiol*. 75:393-422.

An, S.J., C.P. Grabner, and D. Zenisek. 2010. Real-time visualization of complexin during single exocytic events. *Nat Neurosci*. 13:577-583.

Anantharam, A., M.A. Bittner, R.L. Aikman, E.L. Stuenkel, S.L. Schmid, D. Axelrod, and R.W. Holz. 2011. A new role for the dynamin GTPase in the regulation of fusion pore expansion. *Mol Biol Cell*. 22:1907-1918.

Anantharam, A., B. Onoa, R.H. Edwards, R.W. Holz, and D. Axelrod. 2010. Localized topological changes of the plasma membrane upon exocytosis visualized by polarized TIRFM. *J Cell Biol*. 188:415-428.

Anggono, V., K.J. Smillie, M.E. Graham, V.A. Valova, M.A. Cousin, and P.J. Robinson. 2006. Syndapin I is the phosphorylation-regulated dynamin I partner in synaptic vesicle endocytosis. *Nat Neurosci*. 9:752-760.

Ariel, P., and T.A. Ryan. 2012. New insights into molecular players involved in neurotransmitter release. *Physiology (Bethesda)*. 27:15-24.

Ashery, U., N. Bielopolski, B. Barak, and O. Yizhar. 2009. Friends and foes in synaptic transmission: the role of tomosyn in vesicle priming. *Trends Neurosci*. 32:275-282.

Bai, J., Z. Hu, J.S. Dittman, E.C. Pym, and J.M. Kaplan. 2010. Endophilin functions as a membrane-bending molecule and is delivered to endocytic zones by exocytosis. *Cell*. 143:430-441.

Banerjee, A., V.A. Barry, B.R. DasGupta, and T.F. Martin. 1996. N-Ethylmaleimide-sensitive factor acts at a prefusion ATP-dependent step in Ca2+-activated exocytosis. *J Biol Chem*. 271:20223-20226.

Barg, S., M.K. Knowles, X. Chen, M. Midorikawa, and W. Almers. 2010. Syntaxin clusters assemble reversibly at sites of secretory granules in live cells. *Proc Natl Acad Sci U S A*. 107:20804-20809.

Bielopolski, N., A.D. Lam, D. Bar-On, M. Sauer, E.L. Stuenkel, and U. Ashery. 2014. Differential interaction of tomosyn with syntaxin and SNAP25 depends on domains in the WD40 beta-propeller core and determines its inhibitory activity. *J Biol Chem*. 289:17087-17099.

Brauchi, S., G. Krapivinsky, L. Krapivinsky, and D.E. Clapham. 2008. TRPM7 facilitates cholinergic vesicle fusion with the plasma membrane. *Proc Natl Acad Sci U S A*. 105:8304-8308.

Brose, N. 2008. For better or for worse: complexins regulate SNARE function and vesicle fusion. *Traffic*. 9:1403-1413.

Cazares, V.A., M.M. Njus, A. Manly, J.J. Saldate, A. Subramani, Y. Ben-Simon, M.A. Sutton, U. Ashery, and E.L. Stuenkel. 2016. Dynamic Partitioning of Synaptic Vesicle Pools by the SNARE-Binding Protein Tomosyn. *J Neurosci*. 36:11208-11222.

Chang, C.W., C.W. Chiang, and M.B. Jackson. 2017. Fusion pores and their control of neurotransmitter and hormone release. *J Gen Physiol*. 149:301-322.

Choi, S., J. Klingauf, and R.W. Tsien. 2003. Fusion pore modulation as a presynaptic mechanism contributing to expression of long-term potentiation. *Philos Trans R Soc Lond B Biol Sci*. 358:695-705.

Chow, R.H., L. von Ruden, and E. Neher. 1992. Delay in vesicle fusion revealed by electrochemical monitoring of single secretory events in adrenal chromaffin cells. *Nature*. 356:60-63.

Daumke, O., A. Roux, and V. Haucke. 2014. BAR domain scaffolds in dynamin-mediated membrane fission. *Cell*. 156:882-892.

David, C., P.S. McPherson, O. Mundigl, and P. de Camilli. 1996. A role of amphiphysin in synaptic vesicle endocytosis suggested by its binding to dynamin in nerve terminals. *Proc Natl Acad Sci U S A*. 93:331-335.

de Wit, H., Y. Lichtenstein, R.B. Kelly, H.J. Geuze, J. Klumperman, and P. van der Sluijs. 2001. Rab4 regulates formation of synaptic-like microvesicles from early endosomes in PC12 cells. *Mol Biol Cell*. 12:3703-3715.

Fan, F., C. Ji, Y. Wu, S.M. Ferguson, N. Tamarina, L.H. Philipson, and X. Lou. 2015. Dynamin 2 regulates biphasic insulin secretion and plasma glucose homeostasis. *J Clin Invest*. 125:4026-4041.

Felmy, F. 2007. Modulation of cargo release from dense core granules by size and actin network. *Traffic*. 8:983-997.

Ferguson, S.M., and P. De Camilli. 2012. Dynamin, a membrane-remodelling GTPase. *Nat Rev Mol Cell Biol*. 13:75-88.

Fukuda, M. 2008. Regulation of secretory vesicle traffic by Rab small GTPases. *Cell Mol Life Sci*. 65:2801-2813.

Fulop, T., B. Doreian, and C. Smith. 2008. Dynamin I plays dual roles in the activity-dependent shift in exocytic mode in mouse adrenal chromaffin cells. *Arch Biochem Biophys*. 477:146-154.

Gandasi, N.R., and S. Barg. 2014. Contact-induced clustering of syntaxin and munc18 docks secretory granules at the exocytosis site. *Nat Commun*. 5:3914.

Geerts, C.J., R. Mancini, N. Chen, F.T.W. Koopmans, K.W. Li, A.B. Smit, J.R.T. van Weering, M. Verhage, and A.J.A. Groffen. 2017. Tomosyn associates with secretory vesicles in neurons through its N- and C-terminal domains. *PLoS One*. 12:e0180912.

Gonzalez-Jamett, A.M., M.J. Guerra, M.J. Olivares, V. Haro-Acuna, X. Baez-Matus, J. Vasquez-Navarrete, F. Momboisse, N. Martinez-Quiles, and A.M. Cardenas. 2017. The F-Actin Binding Protein Cortactin Regulates the Dynamics of the Exocytotic Fusion Pore through its SH3 Domain. *Front Cell Neurosci*. 11:130.

Gonzalez-Jamett, A.M., F. Momboisse, M.J. Guerra, S. Ory, X. Baez-Matus, N. Barraza, V. Calco, S. Houy, E. Couve, A. Neely, A.D. Martinez, S. Gasman, and A.M. Cardenas. 2013. Dynamin-2 regulates fusion pore expansion and quantal release through a mechanism that involves actin dynamics in neuroendocrine chromaffin cells. *PLoS One*. 8:e70638.

Grabs, D., V.I. Slepnev, Z. Songyang, C. David, M. Lynch, L.C. Cantley, and P. De Camilli. 1997. The SH3 domain of amphiphysin binds the proline-rich domain of dynamin at a single site that defines a new SH3 binding consensus sequence. *J Biol Chem*. 272:13419-13425.

Gracheva, E.O., A.O. Burdina, A.M. Holgado, M. Berthelot-Grosjean, B.D. Ackley, G. Hadwiger, M.L. Nonet, R.M. Weimer, and J.E. Richmond. 2006. Tomosyn inhibits synaptic vesicle priming in Caenorhabditis elegans. *PLoS Biol*. 4:e261.

Graham, M.E., D.W. O'Callaghan, H.T. McMahon, and R.D. Burgoyne. 2002. Dynamin-dependent and dynamin-independent processes contribute to the regulation of single vesicle release kinetics and quantal size. *Proc Natl Acad Sci U S A*. 99:7124-7129.

Guzman, R.E., Y.N. Schwarz, J. Rettig, and D. Bruns. 2010. SNARE force synchronizes synaptic vesicle fusion and controls the kinetics of quantal synaptic transmission. *J Neurosci*. 30:10272-10281.

Haucke, V., and P. De Camilli. 1999. AP-2 recruitment to synaptotagmin stimulated by tyrosine-based endocytic motifs. *Science*. 285:1268-1271.

Heidelberger, R., C. Heinemann, E. Neher, and G. Matthews. 1994. Calcium dependence of the rate of exocytosis in a synaptic terminal. *Nature*. 371:513-515.

Holroyd, P., T. Lang, D. Wenzel, P. De Camilli, and R. Jahn. 2002. Imaging direct, dynamin-dependent recapture of fusing secretory granules on plasma membrane lawns from PC12 cells. *Proc Natl Acad Sci U S A*. 99:16806-16811.

Jahn, R., and D. Fasshauer. 2012. Molecular machines governing exocytosis of synaptic vesicles. *Nature*. 490:201-207.

Jaiswal, J.K., V.M. Rivera, and S.M. Simon. 2009. Exocytosis of post-Golgi vesicles is regulated by components of the endocytic machinery. *Cell*. 137:1308-1319.

Jockusch, W.J., D. Speidel, A. Sigler, J.B. Sorensen, F. Varoqueaux, J.S. Rhee, and N. Brose. 2007. CAPS-1 and CAPS-2 are essential synaptic vesicle priming proteins. *Cell*. 131:796-808.

Kavalali, E.T., and E.M. Jorgensen. 2014. Visualizing presynaptic function. *Nat Neurosci*. 17:10-16.

Kessels, M.M., and B. Qualmann. 2002. Syndapins integrate N-WASP in receptor-mediated endocytosis. *EMBO J*. 21:6083-6094.

Klyachko, V.A., and M.B. Jackson. 2002. Capacitance steps and fusion pores of small and large-dense-core vesicles in nerve terminals. *Nature*. 418:89-92.

Knowles, M.K., S. Barg, L. Wan, M. Midorikawa, X. Chen, and W. Almers. 2010. Single secretory granules of live cells recruit syntaxin-1 and synaptosomal associated protein 25 (SNAP-25) in large copy numbers. *Proc Natl Acad Sci U S A*. 107:20810-20815.

Kuner, T., Y. Li, K.R. Gee, L.F. Bonewald, and G.J. Augustine. 2008. Photolysis of a caged peptide reveals rapid action of N-ethylmaleimide sensitive factor before neurotransmitter release. *Proc Natl Acad Sci U S A*. 105:347-352.

Lang, T., D. Bruns, D. Wenzel, D. Riedel, P. Holroyd, C. Thiele, and R. Jahn. 2001. SNAREs are concentrated in cholesterol-dependent clusters that define docking and fusion sites for exocytosis. *EMBO J*. 20:2202-2213.

Littleton, J.T., R.J. Barnard, S.A. Titus, J. Slind, E.R. Chapman, and B. Ganetzky. 2001. SNARE-complex disassembly by NSF follows synaptic-vesicle fusion. *Proc Natl Acad Sci U S A*. 98:12233-12238.

Liu, Y., and R.H. Edwards. 1997. Differential localization of vesicular acetylcholine and monoamine transporters in PC12 cells but not CHO cells. *J Cell Biol*. 139:907-916.

Liu, Y.W., S. Neumann, R. Ramachandran, S.M. Ferguson, T.J. Pucadyil, and S.L. Schmid. 2011. Differential curvature sensing and generating activities of dynamin isoforms provide opportunities for tissue-specific regulation. *Proc Natl Acad Sci U S A*. 108:E234-242.

Llobet, A., M. Wu, and L. Lagnado. 2008. The mouth of a dense-core vesicle opens and closes in a concerted action regulated by calcium and amphiphysin. *J Cell Biol*. 182:1017-1028.

Logan, T., J. Bendor, C. Toupin, K. Thorn, and R.H. Edwards. 2017. alpha-Synuclein promotes dilation of the exocytotic fusion pore. *Nat Neurosci*. 20:681-689.

Malacombe, M., M.F. Bader, and S. Gasman. 2006. Exocytosis in neuroendocrine cells: new tasks for actin. *Biochim Biophys Acta*. 1763:1175-1183.

Martin, T.F. 2015. PI(4,5)P(2)-binding effector proteins for vesicle exocytosis. *Biochim Biophys Acta*. 1851:785-793.

Martina, J.A., C.J. Bonangelino, R.C. Aguilar, and J.S. Bonifacino. 2001. Stonin 2: an adaptor-like protein that interacts with components of the endocytic machinery. *J Cell Biol*. 153:1111-1120.

McEwen, J.M., J.M. Madison, M. Dybbs, and J.M. Kaplan. 2006. Antagonistic regulation of synaptic vesicle priming by Tomosyn and UNC-13. *Neuron*. 51:303-315.

McMahon, H.T., and E. Boucrot. 2011. Molecular mechanism and physiological functions of clathrin-mediated endocytosis. *Nat Rev Mol Cell Biol*. 12:517-533.

McPherson, P.S., A.J. Czernik, T.J. Chilcote, F. Onofri, F. Benfenati, P. Greengard, J. Schlessinger, and P. De Camilli. 1994. Interaction of Grb2 via its Src homology 3 domains with synaptic proteins including synapsin I. *Proc Natl Acad Sci U S A*. 91:6486-6490.

McPherson, P.S., E.P. Garcia, V.I. Slepnev, C. David, X. Zhang, D. Grabs, W.S. Sossin, R. Bauerfeind, Y. Nemoto, and P. De Camilli. 1996. A presynaptic inositol-5-phosphatase. *Nature*. 379:353-357.

Miesenbock, G., D.A. De Angelis, and J.E. Rothman. 1998. Visualizing secretion and synaptic transmission with pH-sensitive green fluorescent proteins. *Nature*. 394:192-195.

Min, L., Y.M. Leung, A. Tomas, R.T. Watson, H.Y. Gaisano, P.A. Halban, J.E. Pessin, and J.C. Hou. 2007. Dynamin is functionally coupled to insulin granule exocytosis. *J Biol Chem*. 282:33530-33536.

Okamoto, P.M., J.S. Herskovits, and R.B. Vallee. 1997. Role of the basic, proline-rich region of dynamin in Src homology 3 domain binding and endocytosis. *J Biol Chem*. 272:11629-11635.

Pawlu, C., A. DiAntonio, and M. Heckmann. 2004. Postfusional control of quantal current shape. *Neuron*. 42:607-618.

Qualmann, B., J. Roos, P.J. DiGregorio, and R.B. Kelly. 1999. Syndapin I, a synaptic dynamin-binding protein that associates with the neural Wiskott-Aldrich syndrome protein. *Mol Biol Cell*. 10:501-513.

Roos, J., and R.B. Kelly. 1999. The endocytic machinery in nerve terminals surrounds sites of exocytosis. *Curr Biol*. 9:1411-1414.

Ryu, J.K., R. Jahn, and T.Y. Yoon. 2016. Review: Progresses in understanding N-ethylmaleimide sensitive factor (NSF) mediated disassembly of SNARE complexes. *Biopolymers*. 105:518-531.

Sabatini, B.L., and W.G. Regehr. 1996. Timing of neurotransmission at fast synapses in the mammalian brain. *Nature*. 384:170-172.

Samasilp, P., S.A. Chan, and C. Smith. 2012. Activity-dependent fusion pore expansion regulated by a calcineurin-dependent dynamin-syndapin pathway in mouse adrenal chromaffin cells. *J Neurosci*. 32:10438-10447.

Shupliakov, O. 2009. The synaptic vesicle cluster: a source of endocytic proteins during neurotransmitter release. *Neuroscience*. 158:204-210.

Shupliakov, O., P. Low, D. Grabs, H. Gad, H. Chen, C. David, K. Takei, P. De Camilli, and L. Brodin. 1997. Synaptic vesicle endocytosis impaired by disruption of dynamin-SH3 domain interactions. *Science*. 276:259-263.

Sochacki, K.A., B.T. Larson, D.C. Sengupta, M.P. Daniels, G. Shtengel, H.F. Hess, and J.W. Taraska. 2012. Imaging the post-fusion release and capture of a vesicle membrane protein. *Nat Commun*. 3:1154.

Sollner, T., S.W. Whiteheart, M. Brunner, H. Erdjument-Bromage, S. Geromanos, P. Tempst, and J.E. Rothman. 1993. SNAP receptors implicated in vesicle targeting and fusion. *Nature*. 362:318-324.

Stachowiak, J.C., E.M. Schmid, C.J. Ryan, H.S. Ann, D.Y. Sasaki, M.B. Sherman, P.L. Geissler, D.A. Fletcher, and C.C. Hayden. 2012. Membrane bending by protein-protein crowding. *Nat Cell Biol*. 14:944-949.

Stevens, D.R., and J. Rettig. 2009. The Ca(2+)-dependent activator protein for secretion CAPS: do I dock or do I prime? *Mol Neurobiol*. 39:62-72.

Sudhof, T.C. 2013a. A molecular machine for neurotransmitter release: synaptotagmin and beyond. *Nat Med*. 19:1227-1231.

Sudhof, T.C. 2013d. Neurotransmitter release: the last millisecond in the life of a synaptic vesicle. *Neuron*. 80:675-690.

Sudhof, T.C., and J.E. Rothman. 2009. Membrane fusion: grappling with SNARE and SM proteins. *Science*. 323:474-477.

Takamori, S., M. Holt, K. Stenius, E.A. Lemke, M. Gronborg, D. Riedel, H. Urlaub, S. Schenck, B. Brugger, P. Ringler, S.A. Muller, B. Rammner, F. Grater, J.S. Hub, B.L. De Groot, G. Mieskes, Y. Moriyama, J. Klingauf, H. Grubmuller, J. Heuser, F. Wieland, and R. Jahn. 2006. Molecular anatomy of a trafficking organelle. *Cell*. 127:831-846.

Taraska, J.W., D. Perrais, M. Ohara-Imaizumi, S. Nagamatsu, and W. Almers. 2003. Secretory granules are recaptured largely intact after stimulated exocytosis in cultured endocrine cells. *Proc Natl Acad Sci U S A*. 100:2070-2075.

Thomas-Reetz, A.C., and P. De Camilli. 1994. A role for synaptic vesicles in non-neuronal cells: clues from pancreatic beta cells and from chromaffin cells. *FASEB J*. 8:209-216.

Trexler, A.J., K.A. Sochacki, and J.W. Taraska. 2016. Imaging the recruitment and loss of proteins and lipids at single sites of calcium-triggered exocytosis. *Mol Biol Cell*. 27:2423-2434.

Trexler, A.J., and J.W. Taraska. 2017. Two-Color Total Internal Reflection Fluorescence Microscopy of Exocytosis in Endocrine Cells. *Methods Mol Biol*. 1563:151-165.

Trimbuch, T., and C. Rosenmund. 2016. Should I stop or should I go? The role of complexin in neurotransmitter release. *Nat Rev Neurosci*. 17:118-125.

Tsuboi, T., H.T. McMahon, and G.A. Rutter. 2004. Mechanisms of dense core vesicle recapture following "kiss and run" ("cavicapture") exocytosis in insulin-secreting cells. *J Biol Chem*. 279:47115-47124.

Tsuboi, T., and G.A. Rutter. 2003. Multiple forms of "kiss-and-run" exocytosis revealed by evanescent wave microscopy. *Curr Biol*. 13:563-567.

Ullrich, A., M.A. Bohme, J. Schoneberg, H. Depner, S.J. Sigrist, and F. Noe. 2015. Dynamical Organization of Syntaxin-1A at the Presynaptic Active Zone. *PLoS Comput Biol*. 11:e1004407.

Ungermann, C., B.J. Nichols, H.R. Pelham, and W. Wickner. 1998. A vacuolar v-t-SNARE complex, the predominant form in vivo and on isolated vacuoles, is disassembled and activated for docking and fusion. *J Cell Biol*. 140:61-69.

van den Bogaart, G., M.G. Holt, G. Bunt, D. Riedel, F.S. Wouters, and R. Jahn. 2010. One SNARE complex is sufficient for membrane fusion. *Nat Struct Mol Biol*. 17:358-364.

Verhage, M., H.T. McMahon, W.E. Ghijsen, F. Boomsma, G. Scholten, V.M. Wiegant, and D.G. Nicholls. 1991. Differential release of amino acids, neuropeptides, and catecholamines from isolated nerve terminals. *Neuron*. 6:517-524.

Warnock, D.E., J.E. Hinshaw, and S.L. Schmid. 1996. Dynamin self-assembly stimulates its GTPase activity. *J Biol Chem*. 271:22310-22314.

Wen, P.J., S. Grenklo, G. Arpino, X. Tan, H.S. Liao, J. Heureaux, S.Y. Peng, H.C. Chiang, E. Hamid, W.D. Zhao, W. Shin, T. Nareoja, E. Evergren, Y. Jin, R. Karlsson, S.N. Ebert, A. Jin, A.P. Liu, O. Shupliakov, and L.G. Wu. 2016. Actin dynamics provides membrane tension to merge fusing vesicles into the plasma membrane. *Nat Commun*. 7:12604.

Wigge, P., Y. Vallis, and H.T. McMahon. 1997. Inhibition of receptor-mediated endocytosis by the amphiphysin SH3 domain. *Curr Biol*. 7:554-560.

Willig, K.I., S.O. Rizzoli, V. Westphal, R. Jahn, and S.W. Hell. 2006. STED microscopy reveals that synaptotagmin remains clustered after synaptic vesicle exocytosis. *Nature*. 440:935-939.

Woodman, P.G. 2000. Biogenesis of the sorting endosome: the role of Rab5. *Traffic*. 1:695-701.

Wragg, R.T., D. Snead, Y. Dong, T.F. Ramlall, I. Menon, J. Bai, D. Eliezer, and J.S. Dittman. 2013. Synaptic vesicles position complexin to block spontaneous fusion. *Neuron*. 77:323-334.

Wu, L.G., E. Hamid, W. Shin, and H.C. Chiang. 2014. Exocytosis and endocytosis: modes, functions, and coupling mechanisms. *Annu Rev Physiol*. 76:301-331.

Xu, T., and P. Xu. 2008. Searching for molecular players differentially involved in neurotransmitter and neuropeptide release. *Neurochem Res*. 33:1915-1919.

Yamada, H., S. Padilla-Parra, S.J. Park, T. Itoh, M. Chaineau, I. Monaldi, O. Cremona, F. Benfenati, P. De Camilli, M. Coppey-Moisan, M. Tramier, T. Galli, and K. Takei. 2009. Dynamic interaction of amphiphysin with N-WASP regulates actin assembly. *J Biol Chem*. 284:34244-34256.

Yoon, T.Y., X. Lu, J. Diao, S.M. Lee, T. Ha, and Y.K. Shin. 2008. Complexin and Ca2+ stimulate SNARE-mediated membrane fusion. *Nat Struct Mol Biol*. 15:707-713.

Yoshida, Y., M. Kinuta, T. Abe, S. Liang, K. Araki, O. Cremona, G. Di Paolo, Y. Moriyama, T. Yasuda, P. De Camilli, and K. Takei. 2004. The stimulatory action of amphiphysin on dynamin function is dependent on lipid bilayer curvature. *EMBO J*. 23:3483-3491.

Zhang, Z., and M.B. Jackson. 2010. Membrane bending energy and fusion pore kinetics in Ca(2+)-triggered exocytosis. *Biophys J*. 98:2524-2534.

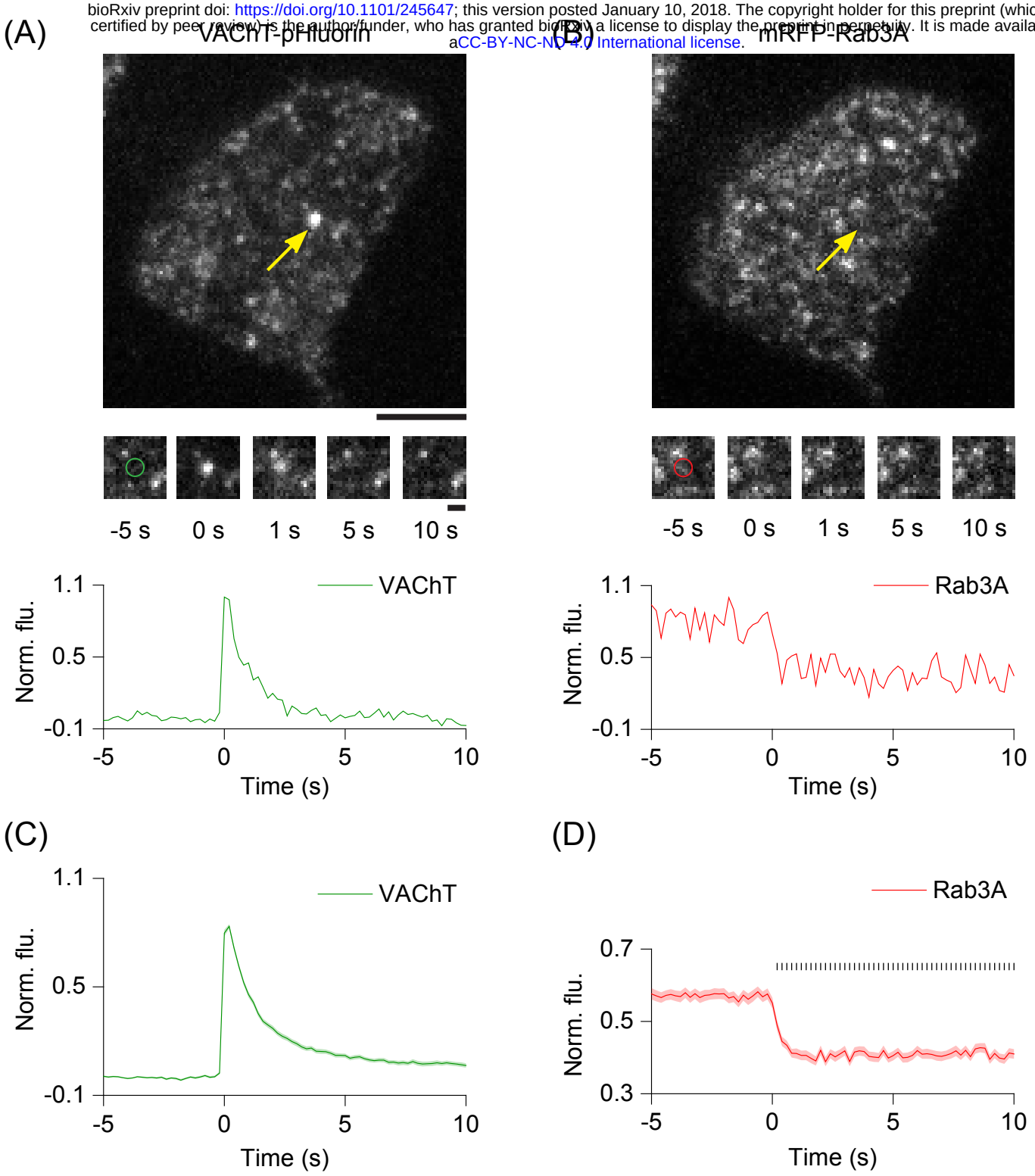

Figure 1. Imaging protein dynamics at SLMV fusion sites in PC12 cells

A, **B**. Image of a PC12 cell transfected with VAChT-pH (**A**) and mRFP-Rab3A (**B**) imaged using TIRF microscopy. Arrows (yellow) show a fusion event in the green channel and the corresponding region in the red channel, after application of stimulation buffer. Scale bar = 5 µm. (Middle) Snapshots of the fusion event shown above at the indicated time-points. '0 s' indicates the manually identified first frame of brightening in the green channel. Circles (~ 1 µm diameter) represent regions used for intensity analysis. Scale bar = 1 µm. (Bottom) Time-lapse traces of normalized fluorescence intensities for the event shown above in the green and red channels. **C, D**. Average time-lapse traces of normalized fluorescence intensities in the green (left) and red (right) channels (196 events, 5 cells). Individual event traces were time-aligned to 0 s, which corresponds to the fusion frame in the green channel. Small vertical black lines in (**D**) indicate $p < 0.01$ (paired Student's t-test) when compared with the average pre-fusion value obtained from -5 to -3s. Standard errors are plotted as shaded areas around the average trace.

Figure 1

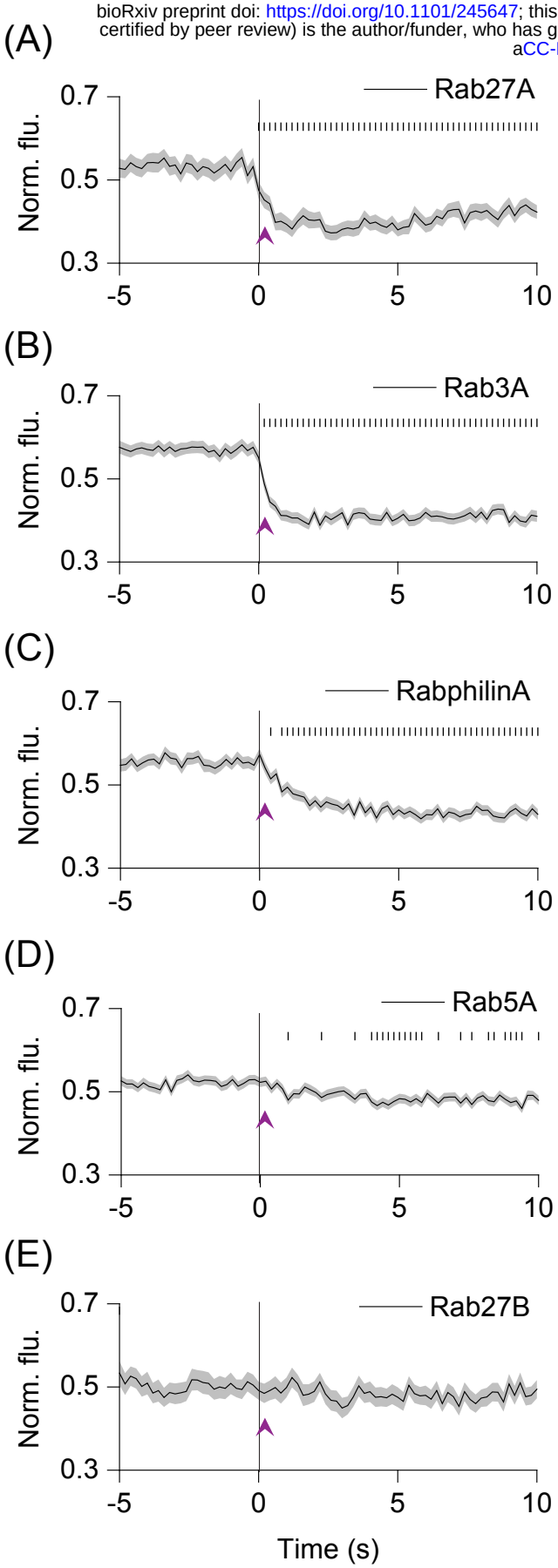

Figure 2. Dynamics of Rab proteins during SLMV fusion

A-E. Average time-lapse traces of normalized fluorescence intensities in the red channel for: **A.** mCherry-Rab27A (103 events, 4 cells); **B**. mRFP-Rab3A (196 events, 5 cells); **C.** mCherry-Rabphilin3A (198 events, 6 cells); **D.** mCherry-Rab27B (73 events, 3 cells); and **E.** mCherry-Rab5A (276 events, 6 cells). Individual event traces were time-aligned to 0 s, which corresponds to the fusion frame in the green channel. Small vertical black lines indicate $p < 0.01$ (paired Student's t-test) when compared with the average pre-fusion value obtained from -5 to – 3 s (horizontal black line). Standard errors are plotted as shaded areas around the average trace. Arrowheads indicate approximate time-points from where average 'Fusion' images were obtained for Supp. Fig. 2.

Figure 2

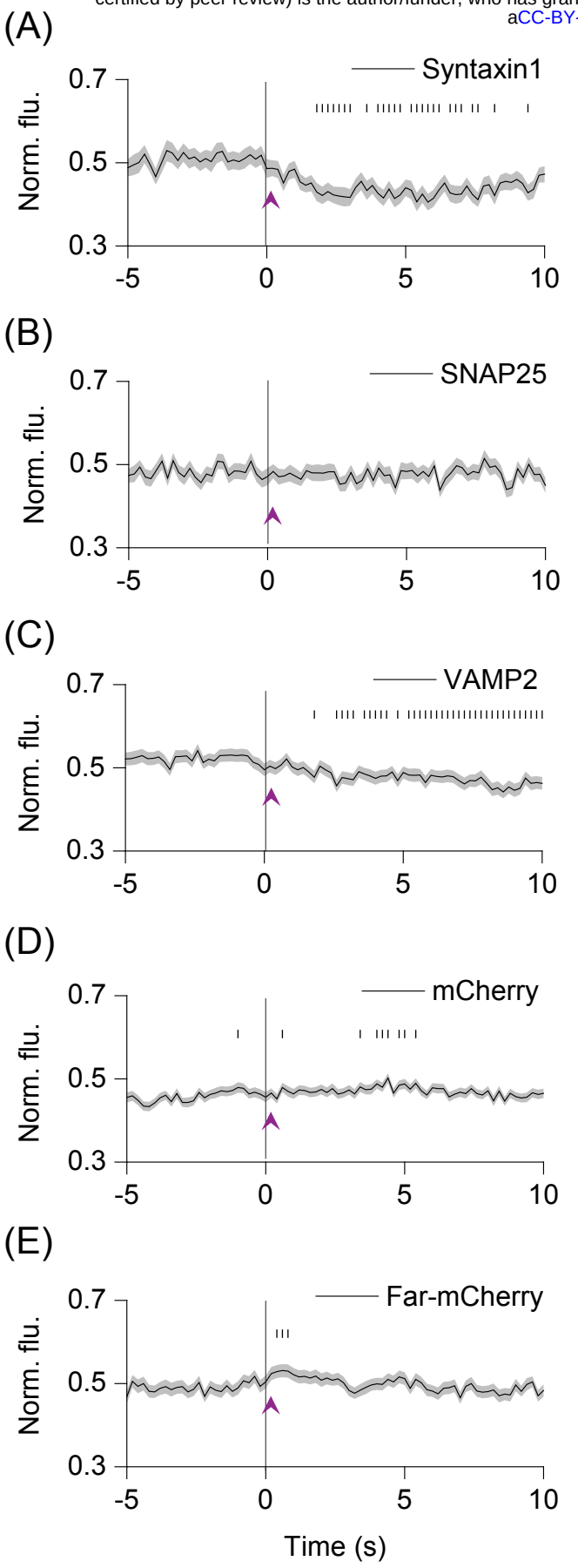

Figure 3. **SNAREs syntaxin1 and VAMP2 diffuse away from sites of SLMV fusion**

A-E. Average time-lapse traces of normalized fluorescence intensities in the red channel for: **A.** dCMV-mCherry-syntaxin1 (76 events, 4 cells); **B.** dCMV-mCherry-SNAP25 (97 events, 8 cells); **C.** VAMP2- mCherry (172 events, 7 cells); **D.** mCherry (274 events, 8 cells); and **E.** farnesyl-mCherry (166 events, 9 cells). Individual event traces were time-aligned to 0 s, which corresponds to the fusion frame in the green channel. Small vertical black lines indicate $p < 0.01$ (paired Student's t-test) when compared with the average pre-fusion value obtained from -5 to – 3s. Standard errors are plotted as shaded areas around the average trace. Arrowheads indicate approximate time-points from where average 'Fusion' images were obtained for Supp. Fig. 2.

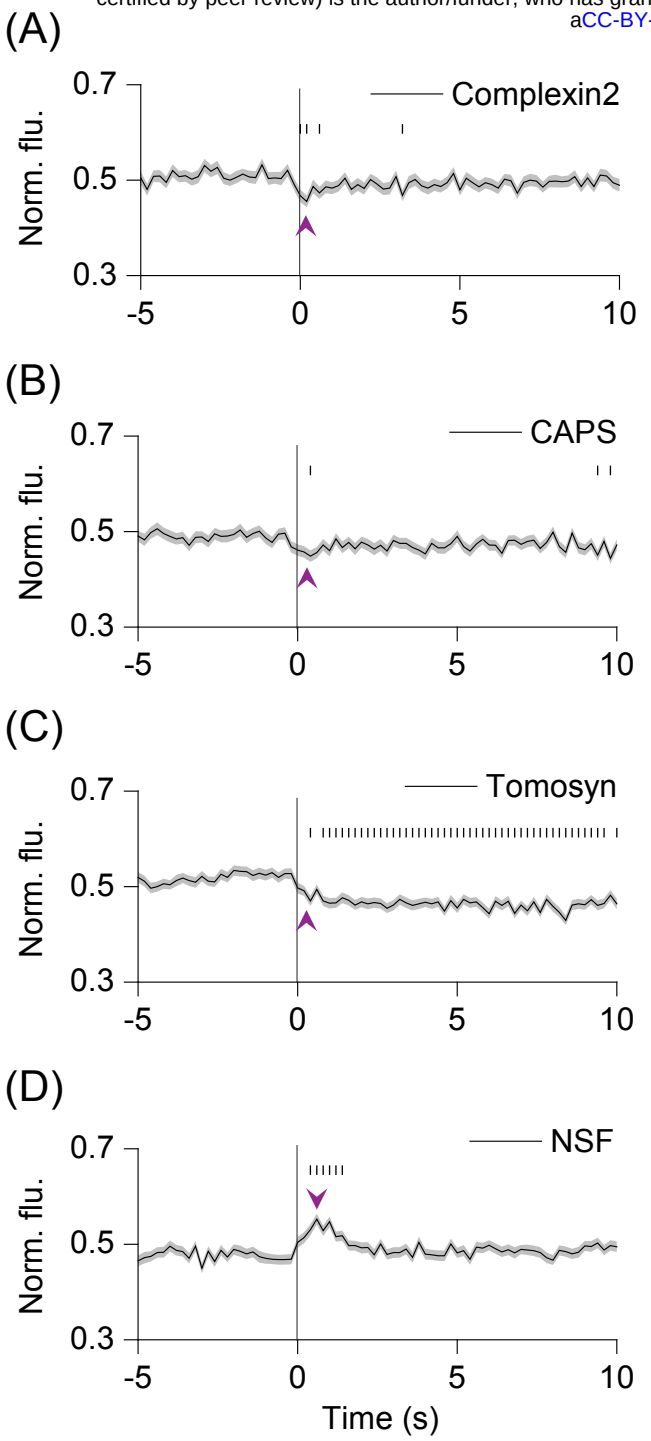

Figure 4. **SNARE modulators exhibit diverse behaviors during fusion**

A-C. Average time-lapse traces of normalized fluorescence intensities in the red channel for: **A.** complexin2-mCherry (202 events, 7 cells); **B.** CAPS-mKate2 (232 events, 5 cells); **C.** mCherry-tomosyn (289 events, 9 cells); and **D.** NSF-mCherry (274 events, 5 cells). Individual event traces were time-aligned to 0 s, which corresponds to the fusion frame in the green channel. Small vertical black lines indicate $p < 0.01$ (paired Student's t-test) when compared with the average pre-fusion value obtained from -5 to –3 s (horizontal black line). Standard errors are plotted as shaded areas around the average trace. Arrowheads indicate approximate time-points from where average 'Fusion' images were obtained for Supp. Fig. 2.

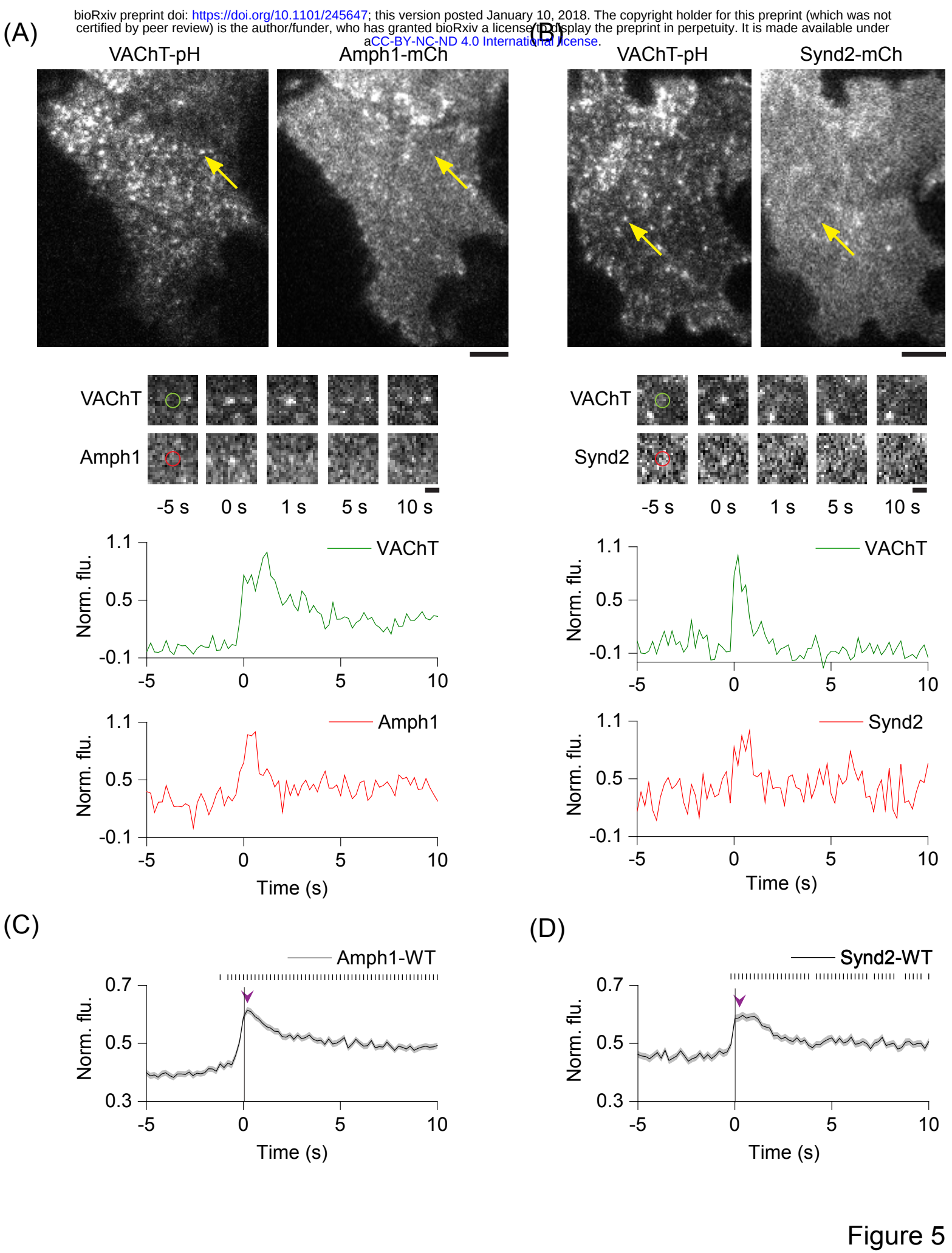

Figure 5

Figure 5. Amphiphysin1 and syndapin2 are transiently recruited to SLMV fusion sites
A, B. Images of PC12 cells expressing (**A**) VAChT-pH (left) and Amphiphysin1-mCherry (right) or (**B**) VAChT-pH (left) and Syndapin2-mCherry (right). Arrowheads show fusion events in the green channel and the corresponding regions in the red channel, after application of stimulation buffer. Scale bar = 5 μm. (Middle) Snapshots of the fusion event shown above at the indicated time-points. Time-point '0' indicates the manually identified first frame of brightening in the green channel. (Bottom) Time-lapse traces of normalized fluorescence intensities in the green and red channels for the single fusion event shown above. **C, D**. Average time-lapse traces of normalized fluorescence intensities in the red channel for Amph1-WT (C, 371 events, 9 cells) and Synd2-WT (228 events, 6 cells). Individual event traces were time-aligned to 0 s, which corresponds to the fusion frame in the green channel. Small vertical black lines in indicate $p < 0.01$ (paired Student's t-test) when compared with the average pre-fusion value obtained from -5 to -3s. Standard errors are plotted as shaded areas around the average trace. Arrowheads indicate approximate time-points from where average 'Fusion' images were obtained for Supp. Fig. 9.

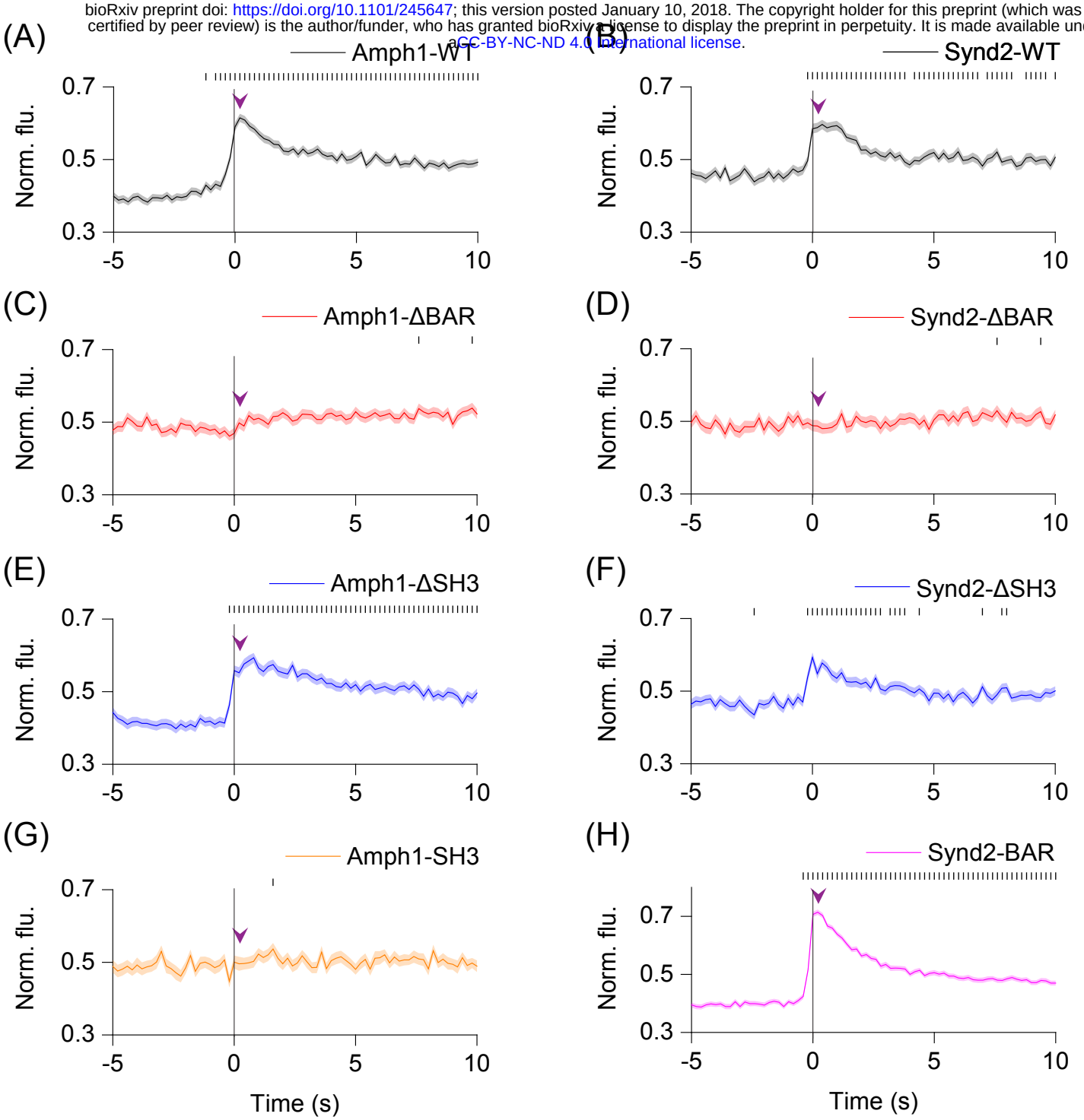

Figure 6. Amphiphysin1 and syndapin2 recruitment is dependent on the BAR domain
A-H. Average time-lapse traces of normalized fluorescence intensities in the red channel for: **A.** Amph1-WT (371 events, 9 cells); **B**. Synd2-WT (228 events, 6 cells); **C**. Amph1-ΔBAR (169 events, 4 cells); **D.** Synd2-ΔBAR (136 events, 11 cells); **E.** Amph1-ΔSH3 (214 events, 13 cells); **F**. Synd2-ΔSH3 (184 events, 9 cells); **G**. Amph1-SH3 (117 events, 8 cells); and **H.** Synd2-BAR (418 events, 13 cells). Individual event traces were time-aligned to 0 s, which corresponds to the fusion frame in the green channel. Small vertical black lines indicate $p < 0.01$ (paired Student's t-test) when compared with the average pre-fusion value obtained from -5 to – 3 s. Standard errors are plotted as shaded areas around the average trace. Arrowheads indicate approximate time-points from where average 'Fusion' images were obtained for Supp. Fig. 9.

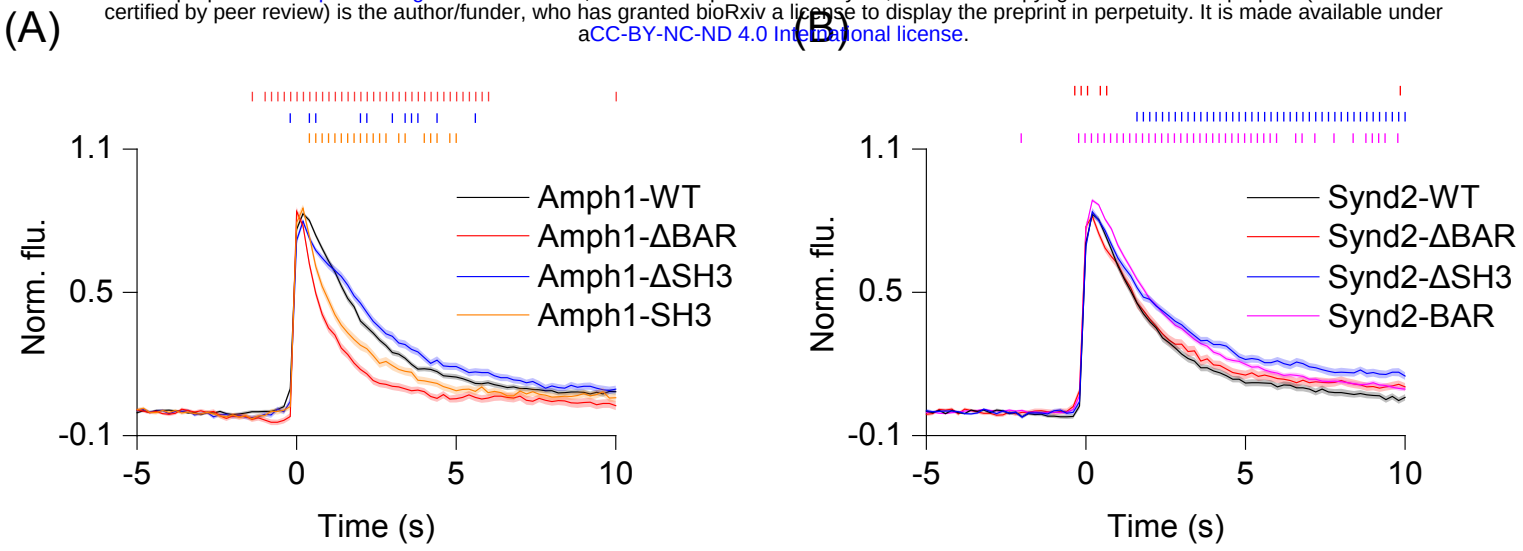

Figure 7. Amphiphysin1 and syndapin2 mutants slow VAChT-pH release

A. Average time-lapse traces of normalized VAChT-pH fluorescence intensities in PC12 cells co-expressed with WT and mutant amphiphysin1 constructs. Colored vertical lines indicate $p < 0.05$ (Student's t-test), when comparing Amph1-ΔBAR (red), Amph1-ΔSH3 (blue), or Amph1-SH3 (orange) with Amph1-WT (black). **B.** Average time-lapse traces of normalized VAChT-pH fluorescence intensities in PC12 cells co-expressed with WT and mutant syndapin2 constructs. Colored vertical lines indicate $p < 0.01$ (Student's t-test), comparing each mutant (Synd2-ΔBAR, red; Synd2-ΔSH3, blue; Synd2-BAR, pink) with Synd2-WT (black). Individual event traces were time-aligned to 0 s, which corresponds to the manually identified first frame of fusion. Standard errors are plotted as shaded areas around the average trace. The same dataset as in Fig. 6 was used.

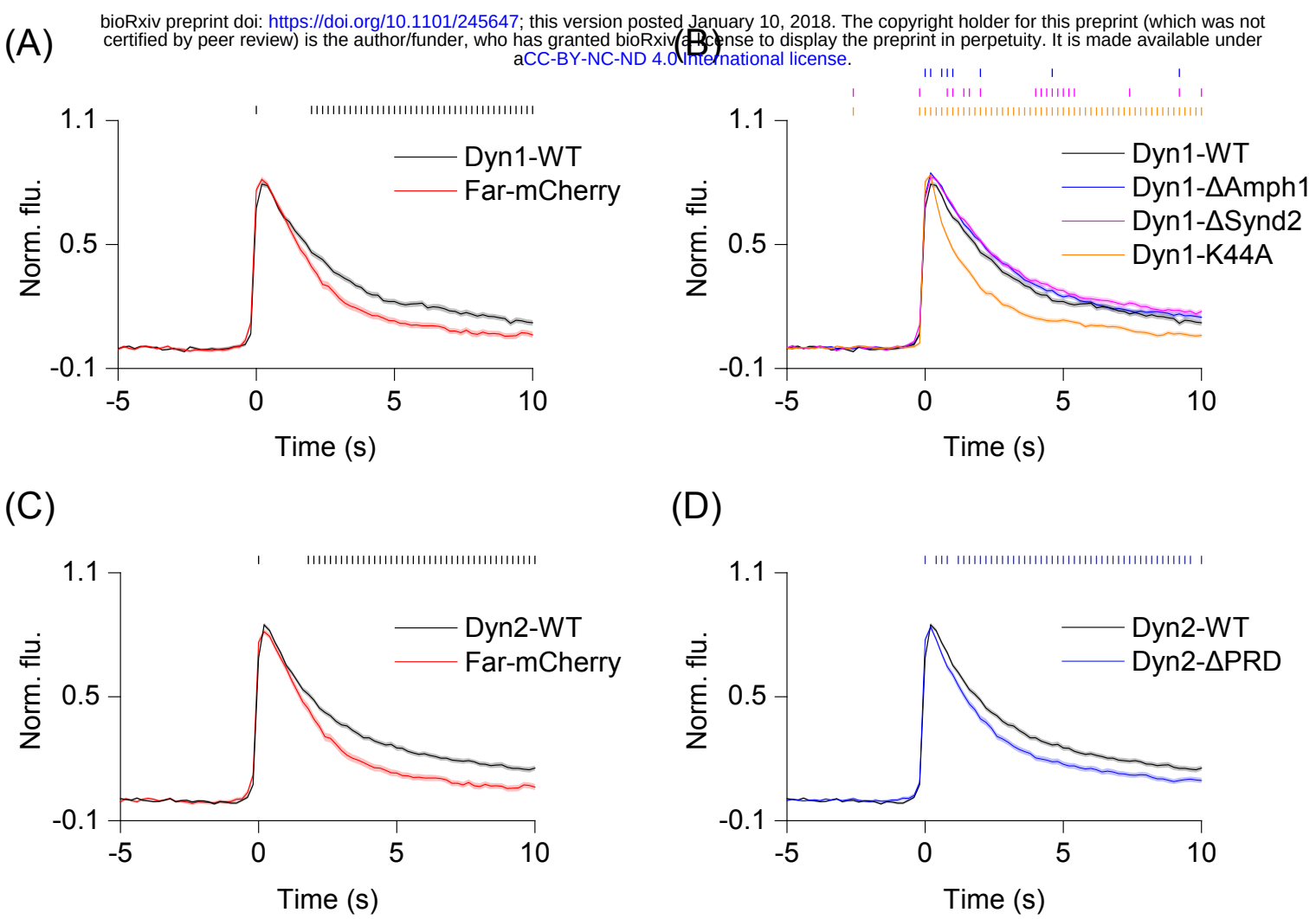

Figure 8. Dynamin1 and dynamin2 slow VAChT-pH release

A-D. Average time-lapse traces of normalized VAChT-pH fluorescence intensities in PC12 cells co-expressed with WT and mutant dynamin1 and dynamin2 constructs. Colored vertical lines indicate $p < 0.01$ (Student's t-test), when comparing: **A**. Dyn1-WT (black) with farnesyl mCherry (red); **B**. Dyn1-K44A (orange), Dyn1-ΔAmph1 (blue), Dyn1-ΔSynd2 (pink) with Dyn1-WT (black); **C**. Dyn2-WT (black) with farnesyl-mCherry (red); and **D**. Dyn2-WT (black) with Dyn2-ΔPRD (blue). Standard errors are plotted as shaded areas around the average trace. The same dataset as in Supp. Fig. 9 was used.

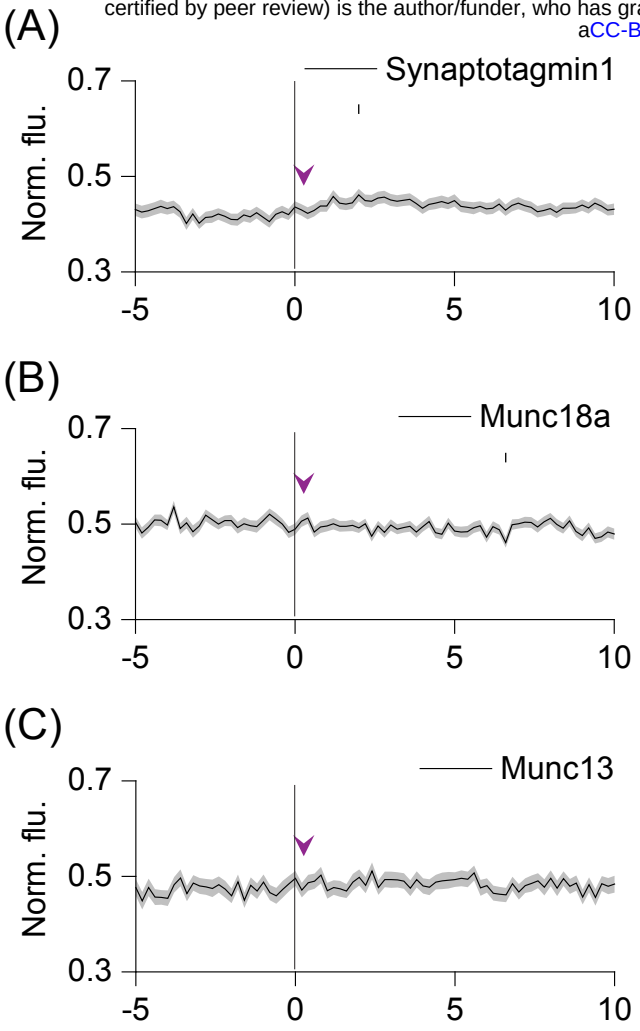

Supplementary Figure 1. Dynamics of SNARE modulators during SLMV fusion

A-D. Average time-lapse traces of normalized fluorescence intensities in the red channel for: **A.** synaptotagmin1-mCherry (266 events, 5 cells); **B.** mCherry-Munc18a (250 events, 11 cells); and **C.** Munc13-mCherry (132 events, 5 cells). Individual event traces were time-aligned to 0 s, which corresponds to the fusion frame in the green channel. Small vertical black lines indicate $p < 0.01$ (paired Student's t-test) when compared with the average pre-fusion value obtained from -5 to – 3s. Standard errors are plotted as shaded areas around the average trace. Arrowheads indicate approximate time-points from where average 'Fusion' images were obtained for Supp. Fig. 2.

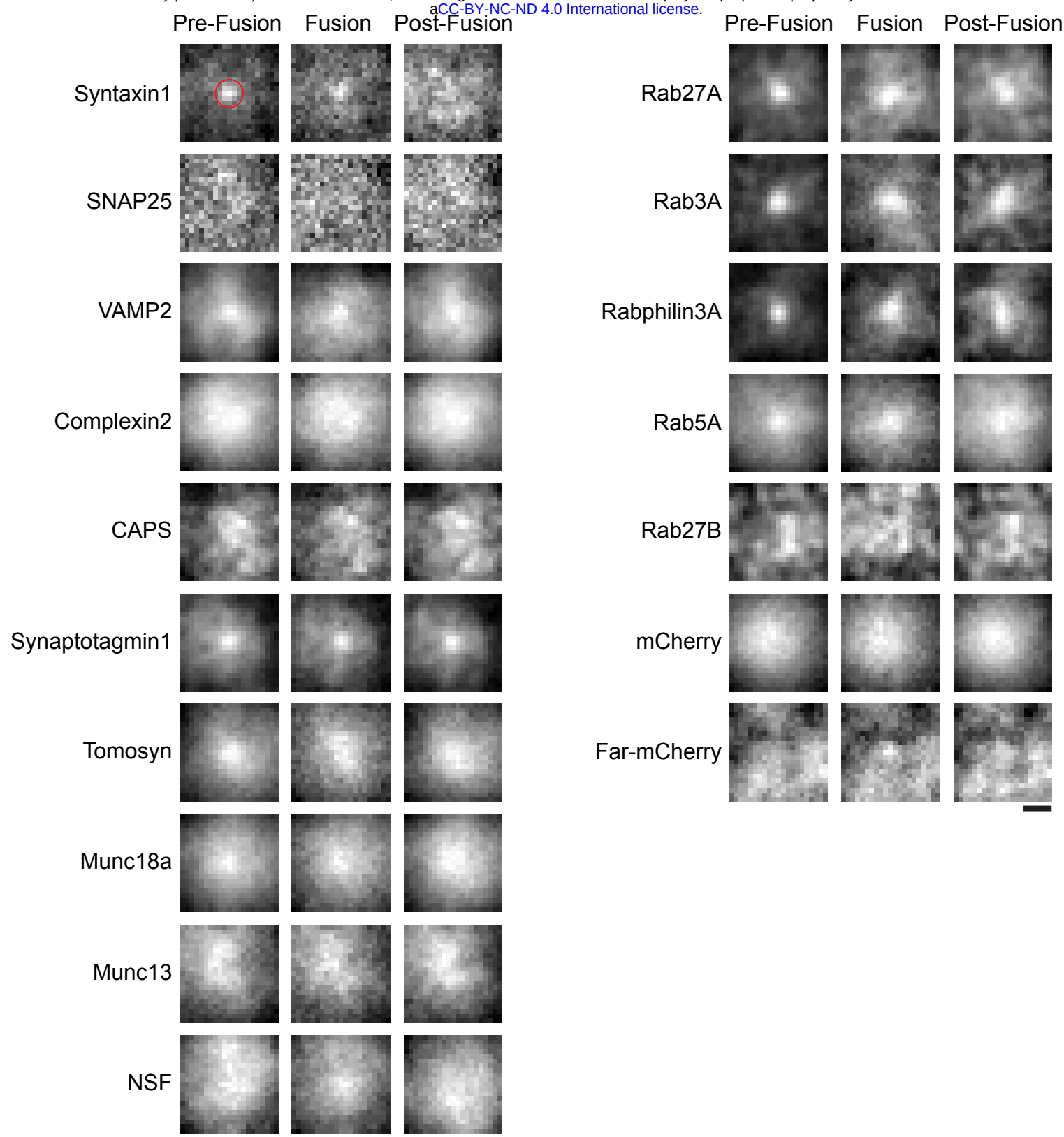

Supplementary Figure 2. Distribution of exocytic proteins at SLMV fusion sites
Images show distribution of red proteins obtained by averaging frames from before (Pre-Fusion, -5 s to -4 s), during (Fusion), and after fusion (Post-Fusion, 4 s to 5 s). Images are normalized to show relative pixel intensities within each image, and therefore intensities cannot be compared across images. Circle (~ 1 μm diameter) represents region used for time-lapse intensity analysis. Scale bar = 1 μm.

Supp Figure 2

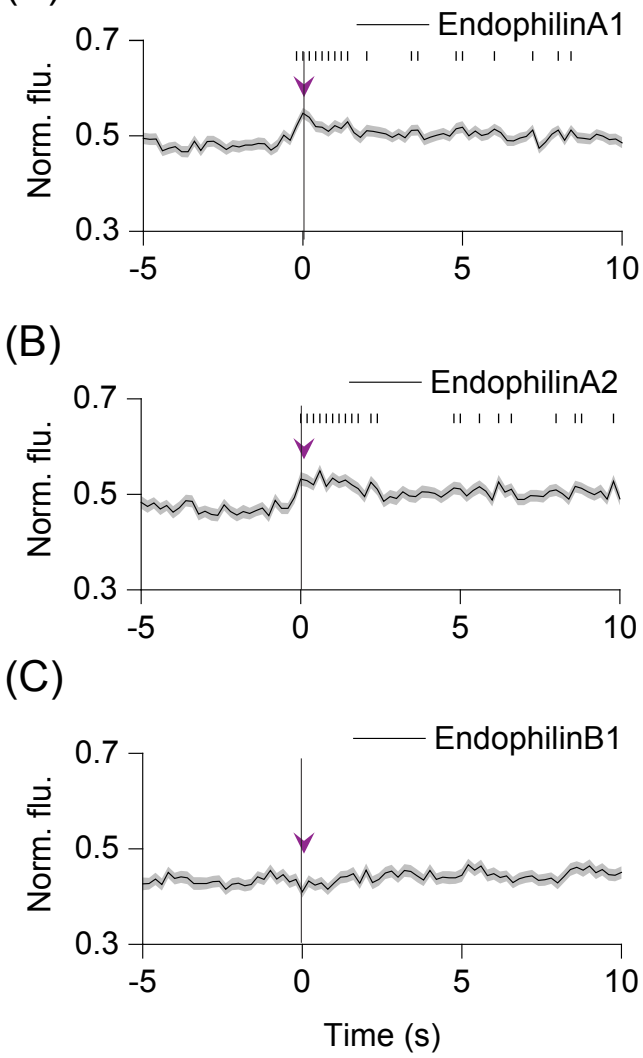

Supplementary Figure 3. Endophilins are localized at SLMV fusion sites during exocytosis

A-C. (Left) Average time-lapse traces of normalized fluorescence intensities in the red channel for: **A**. endophilinA1-mCherry (258 events, 13 cells); **B.** endophilinA2-mCherry (207 events, 11 cells); and **C.** endophilinB1-mCherry (213 events, 11 cells). Individual event traces were time-aligned to 0 s, which corresponds to the fusion frame in the green channel. Small vertical black lines indicate $p < 0.01$ (paired Student's t-test) when compared with the average pre-fusion value obtained from -5 to – 3 s. Standard errors are plotted as shaded areas around the average trace. Arrowheads indicate approximate time-points from where average 'Fusion' images were obtained for Supp. Fig. 9.

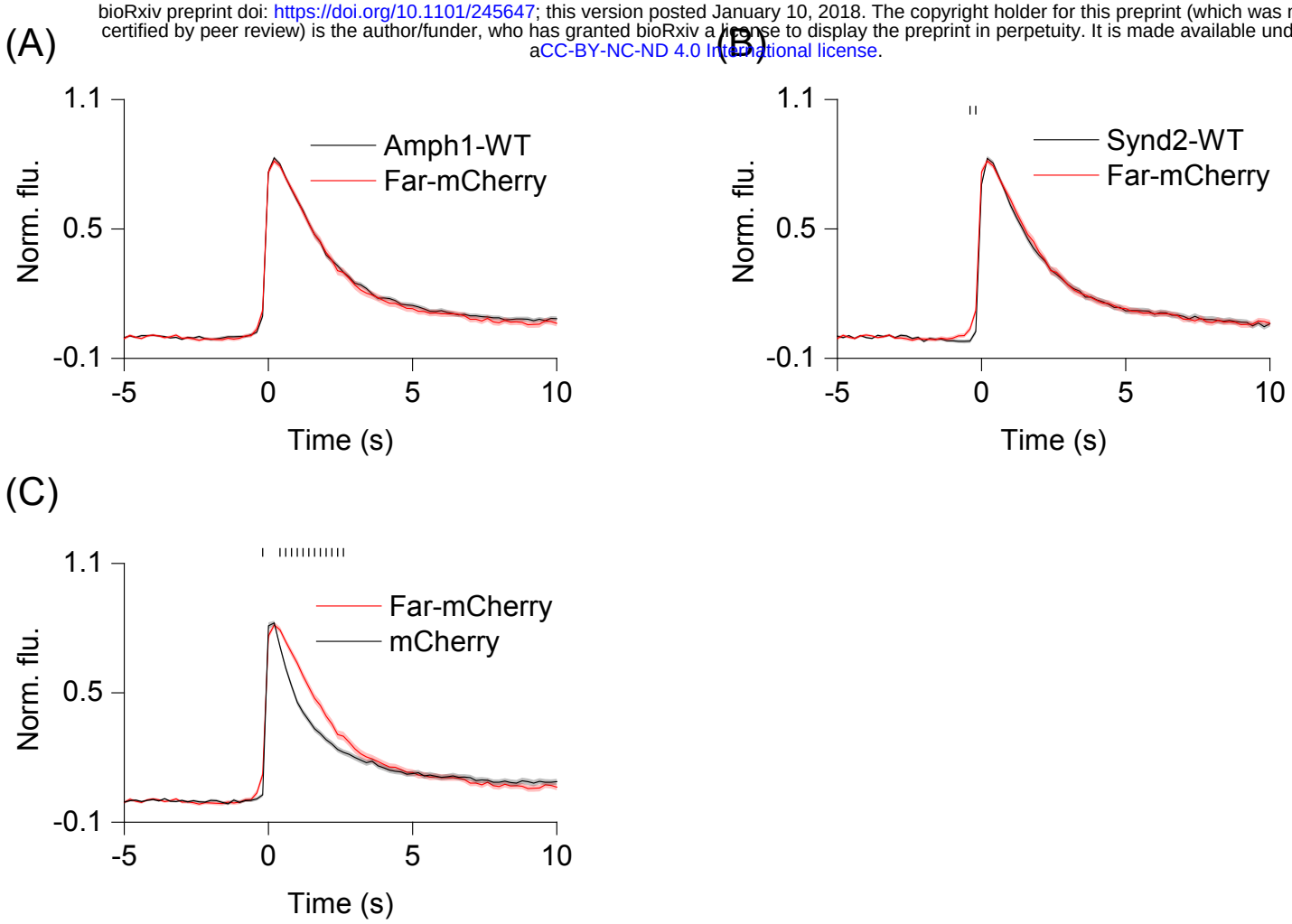

Supplementary Figure 4. VAChT-pH decay in PC12 cells expressing amphiphysin1 and syndapin2

A-C. Average time-lapse traces of normalized VAChT-pH fluorescence intensities when co-expressed with **A.** WT amphiphysin1 (black) or farnesyl-mCherry (red), **B.** WT syndapin2 (black) or farnesyl-mCherry (red), and **C.** mCherry (black) or farnesyl-mCherry (red). Individual traces were time-aligned to 0 s, which corresponds to the manually identified first frame of fusion. Small vertical black lines indicate $p < 0.01$ (Student's t-test). Standard errors are plotted as shaded areas around the average trace.

(A)

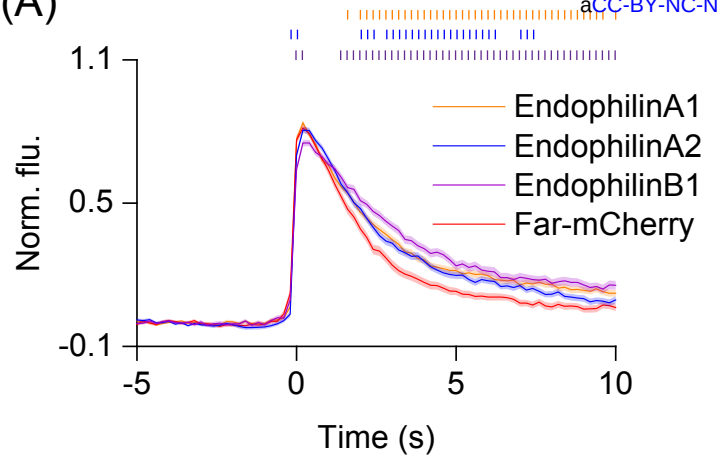

Supplementary Figure 5. Endophilins slow VAChT-pH release

A. Average time-lapse traces of normalized VAChT-pH fluorescence intensities when co-expressed with endophilin constructs. Colored vertical lines indicate $p < 0.01$ (Student's t-test), when comparing endophilinA1 (orange), endophilinA2 (blue), or endophilinB1 (purple) with farnesyl-mCherry (red). Individual traces were time-aligned to 0 s, which corresponds to the manually identified first frame of fusion. Standard errors are plotted as shaded areas around the average trace. The same dataset as in Supp. Fig. 3 was used.

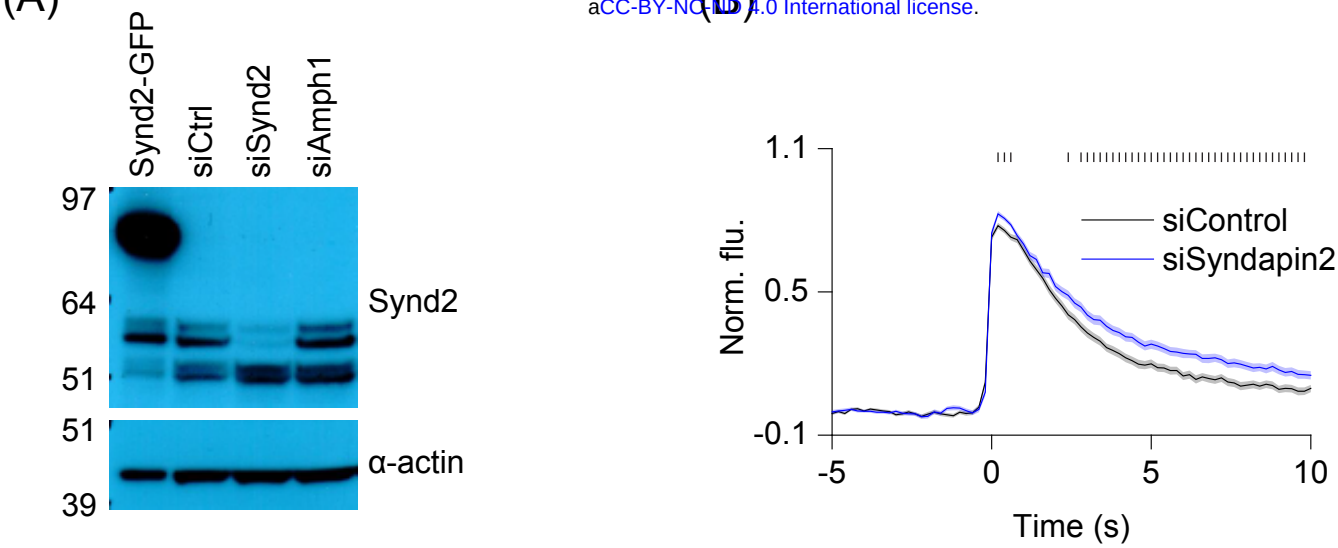

Supplementary Figure 6. Effect of syndapin2 knock-down on VAChT-pH release
A. Western blots showing expression of syndapin2 in PC12 cells that is reduced following treatment with siRNA. (Top) Blot probed with anti-syndapin2 antibody. (Bottom) Same blot re-probed with anti-α-actin. **B.** Average time-lapse traces of normalized VAChT-pH fluorescence intensities in cells treated with control siRNA (black, 219 events, 15 cells) or siSyndapin2 (blue, 184 events, 16 cells). Individual traces were time-aligned to 0 s, which corresponds to the manually identified first frame of fusion. Small blue vertical lines indicate $p < 0.01$ (Student's t-test). Standard errors are plotted as shaded areas around the average trace.

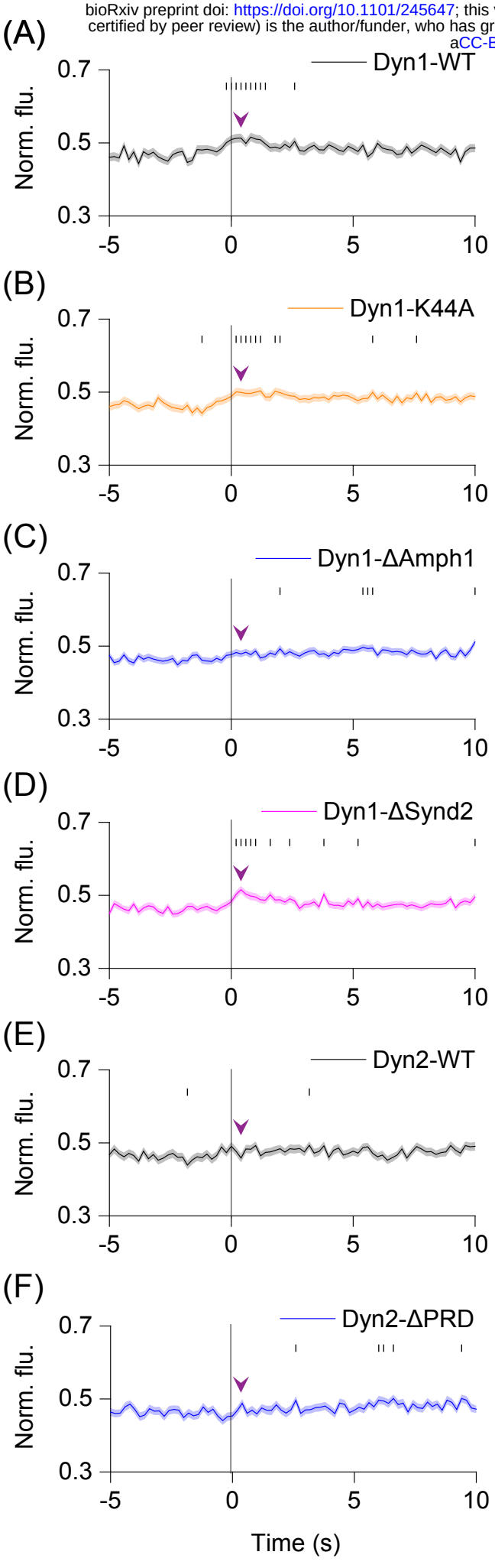

Supplementary Figure 7. Recruitment of WT and mutant dynamin to SLMV fusion sites

A-F. Average time-lapse traces of normalized fluorescence intensities in the red channel for: **A.** Dynamin1-WT (250 events, 14 cells); **B.** Dynamin-K44A (309 events, 12 cells); **C.** Dynamin1-ΔAmph1 (365 events, 17 cells); **D.** Dynamin1-ΔSynd2 (341 events, 17 cells); **E.** Dynamin2-WT (260 events, 12 cells); and **F.** Dynamin2-ΔPRD (252 events, 14 cells). Individual event traces were time-aligned to 0 s, which corresponds to the fusion frame in the green channel. Small vertical black lines indicate $p < 0.01$ (paired Student's t-test) when compared with the average pre-fusion value obtained from -5 to – 3 s. Standard errors are plotted as shaded areas around the average trace. Arrowheads indicate approximate time-points from where average 'Fusion' images were obtained for Supp. Fig. 9.

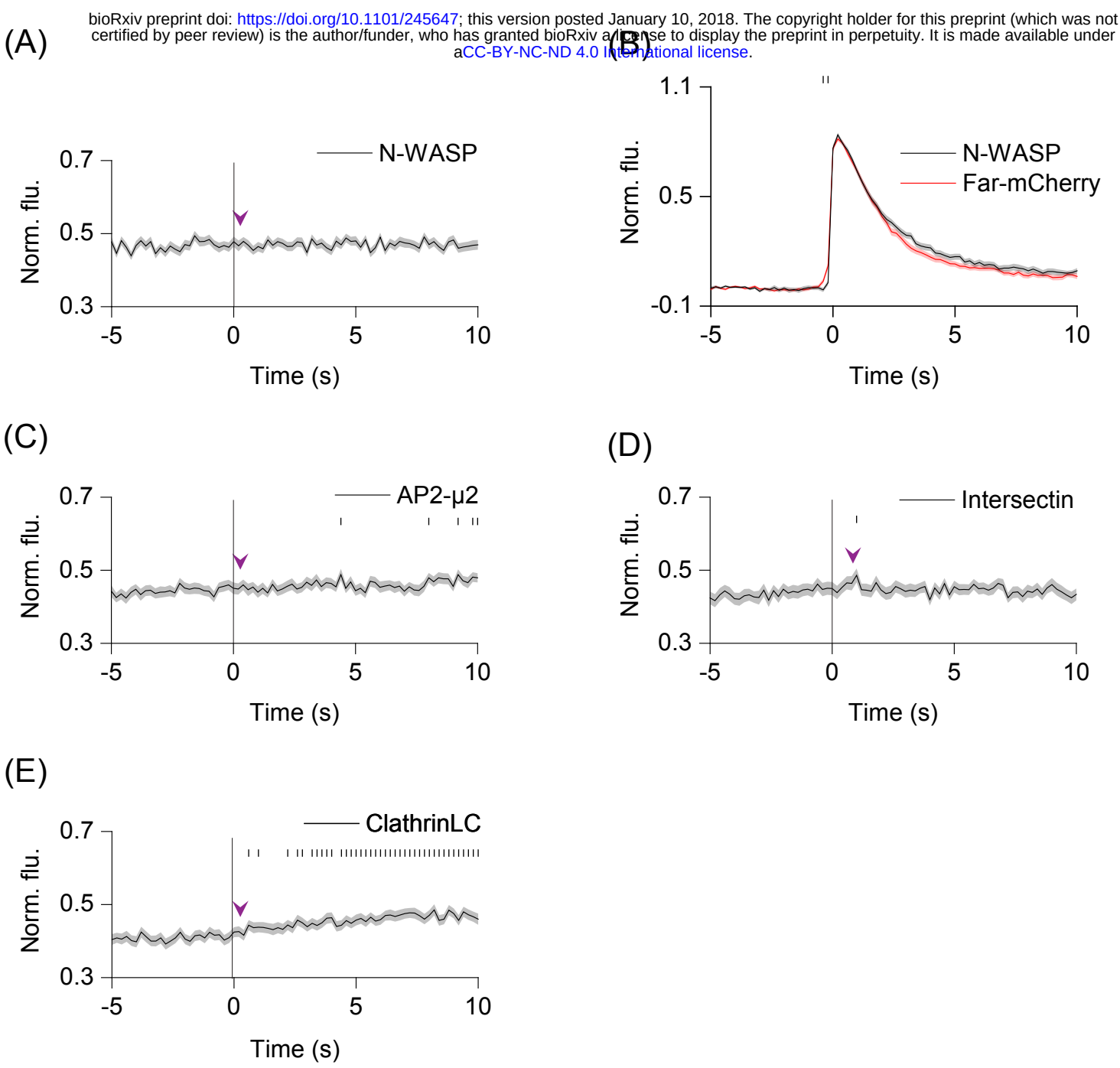

Supplementary Figure 8. Dynamics of other endocytic proteins at SLMV fusion sites
A. Average time-lapse traces of normalized fluorescence intensities in the red channel for NWASP-mCherry (197 events, 8 cells). **B.** Average time-lapse traces of normalized VAChT-pH fluorescence intensities when co-expressed with N-WASP. **C-E.** Average time-lapse traces of normalized fluorescence intensities in the red channel for **C.** AP2- μ2-mCherry (153 events, 5 cells); **D.** Intersectin (122 events, 5 cells); and **E.** ClathrinLC-mCherry (209 events, 5 cells). Individual event traces were time-aligned to 0 s, which corresponds to the fusion frame in the green channel. Small vertical black lines indicate $p < 0.01$ (Student's t-test; paired (**A**, **C-E**), unpaired (**B**)). Standard errors are plotted as shaded areas around the average trace. Arrowheads indicate approximate time-points from where average 'Fusion' images were obtained for Supp. Fig. 9.

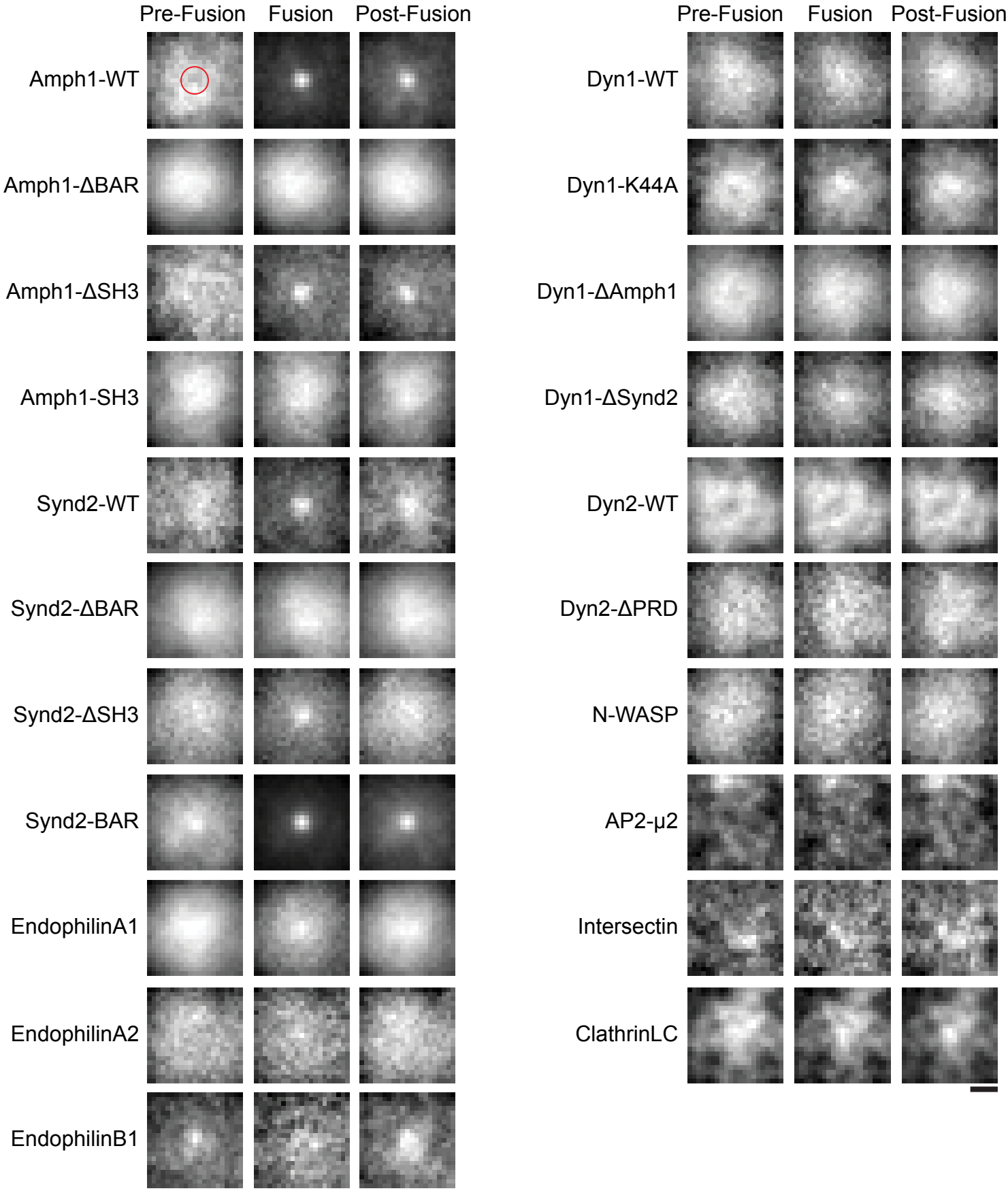

Supplementary Figure 9. Distribution of endocytic proteins at SLMV fusion sites
Images show distribution of red proteins obtained by averaging frames from before (Pre-Fusion, -5 s to -4 s), during (Fusion) and after fusion (Post-Fusion, 4 s to 5 s). Images are normalized to show relative pixel intensities within each image, and therefore intensities cannot be compared across images. Circle (~ 1 μm diameter) represents region used for time-lapse intensity analysis. Scale bar = 1 μm.

Supp Figure 9

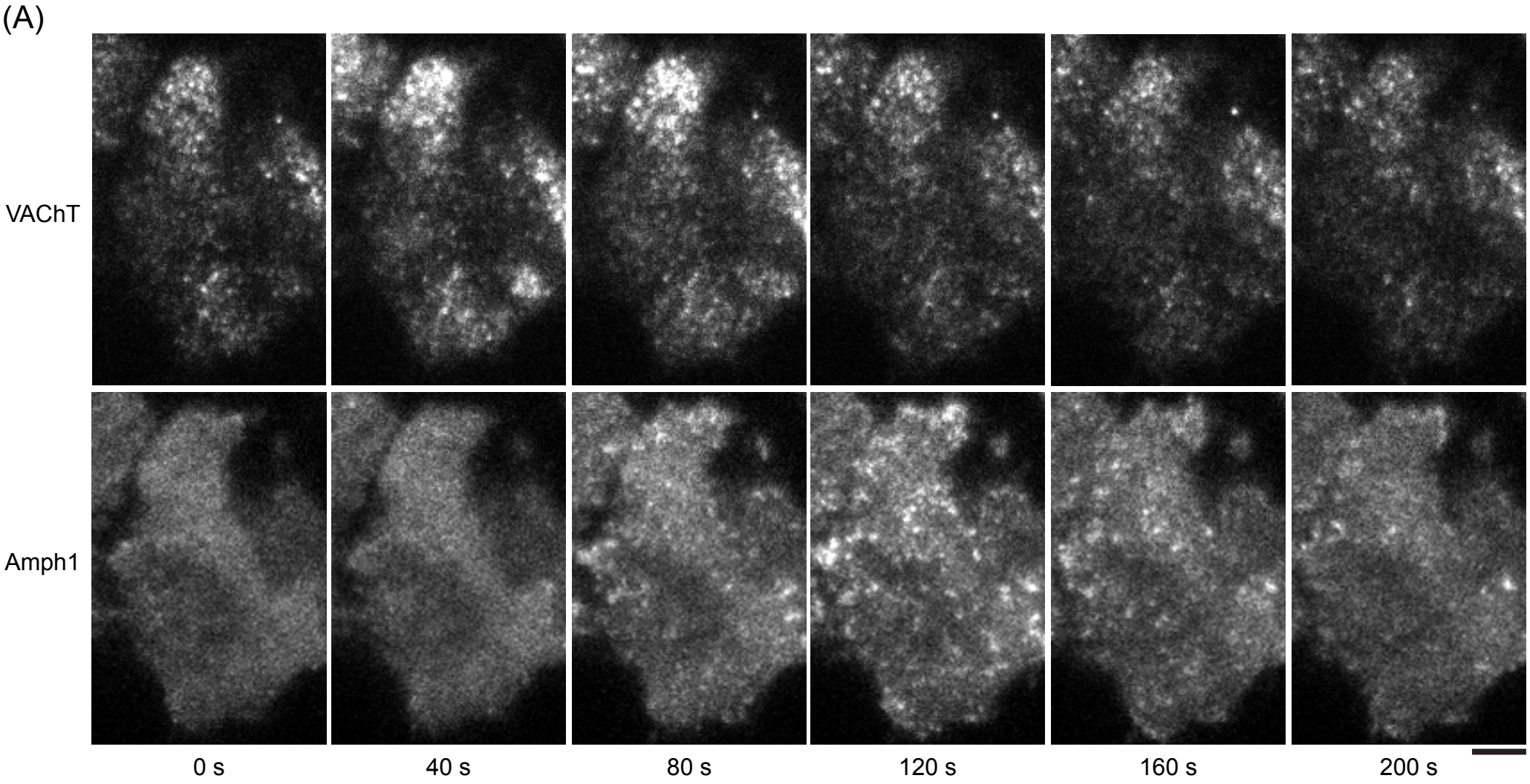

Supplementary Figure 10. Amphiphysin1 recruitment following fusion

A. Images of a PC12 cell expressing VAChT-pH (top) and Amph1-mCherry (bottom) at indicated time-points, with '0 s' being the start of the experiment. Stimulation buffer was applied from ~ 20 s to ~ 50 s. Scale bar = 5 µm. **B.** Time-lapse traces showing background-subtracted and normalized mean fluorescence intensities from a region around the whole cell in the green and red channels.

Supp Figure 10

Supplemental Table 1. List of DNA constructs, cDNA sources, and n values

DNA Construct	No. of Events	No. of Cells	Source of cDNA
VAChT-pHluorin			D. Clapham (Janelia)
dCMV-mCherry-Syntaxin1a*	76	4	W. Almers (OHSU)
dCMV-mCherry-SNAP25*	97	8	J. Taraska (NHLBI/NIH)
VAMP2-mCherry	172	7	R. Scheller (Stanford U.)
mCherry	274	8	Clontech
Farnesyl-mCherry	166	9	J. Taraska (NHLBI/NIH)
Complexin2-mCherry	202	7	Biobasic synthesis
CAPS-mKate2	232	5	T. Martin (UW, Madison)
mCherry-Tomosyn	289	9	Biobasic synthesis
NSF-mCherry	274	5	P. Hanson (Wash U.)
Synaptotagmin1-mCherry	266	5	J. Taraska (NHLBI/NIH)
mCherry-Munc18a	250	11	Biobasic synthesis
Munc13-mCherry	132	5	Biobasic synthesis
mCherry-Rab27A	103	4	W. Westbroek (NIH)
mRFP-Rab3A	196	5	M. Fukuda (Tohoku U.)
mCherry-Rabphilin3A	198	6	I. Macara (Vanderbilt U.)
mCherry-Rab5A	276	6	C. Merrifield (Addgene 27681)
mCherry-Rab27B	73	3	J. Taraska (NHLBI/NIH)
Amphiphysin1-mCherry	371	9	C. Merrifield (Addgene 27692)
Amphiphysin1-ΔBAR-mCherry	169	4	J. Taraska (NHLBI/NIH)
Amphiphysin1-ΔSH3-mCherry	214	13	J. Taraska (NHLBI/NIH)
Amphiphysin1-SH3-mCherry	117	8	J. Taraska (NHLBI/NIH)
mCherry-Syndapin2	228	6	C. Merrifield (Addgene 27681)
mCherry-Syndapin2-ΔBAR	136	11	J. Taraska (NHLBI/NIH)
mCherry-Syndapin2-BAR	418	13	J. Taraska (NHLBI/NIH)
mCherry-Syndapin2-ΔSH3	184	9	J. Taraska (NHLBI/NIH)
EndophilinA1-mCherry	258	13	DNASU HsCD00000899
EndophilinA2-mCherry	207	11	DNASU HsCD00005501
EndophilinB1-mCherry	213	11	DNASU HsCD00042012
Dynamin1-mCherry	250	14	C. Merrifield (Addgene 27697)
Dynamin1-K44A-mCherry	309	12	J. Taraska (NHLBI/NIH)
Dynamin1-833-838A-mCherry	365	17	J. Taraska (NHLBI/NIH)
Dynamin1-S774E/S778E-mCherry	341	17	J. Taraska (NHLBI/NIH)
Dynamin2-mCherry	260	12	C. Merrifield (Addgene 27689)
Dynamin2-ΔPRD-mCherry	252	14	J. Taraska (NHLBI/NIH)
mCherry-N-WASP	197	8	H. Yamada (Okayama U.)
AP2-μ2-mCherry	153	5	C. Merrifield (Addgene 27672)
mCherry-Intersectin	122	5	Peter McPherson (McGill U.)
Clathrin Light Chain-mCherry	209	5	W. Almers (OHSU)
Total	**8249**	**324**	
Average	**217.08**	**8.53**	

*Truncated CMV promoter